

This is an Open Access document downloaded from ORCA, Cardiff University's institutional repository: <https://orca.cardiff.ac.uk/id/eprint/74872/>

This is the author's version of a work that was submitted to / accepted for publication.

Citation for final published version:

Griemsmann, S., Hoft, S. P., Bedner, P., Zhang, J., von Staden, E., Beinhauer, A., Degen, J., Dublin, P., Cope, D. W., Richter, N., Crunelli, Vincenzo, Jabs, R., Willecke, K., Theis, M., Seifert, G., Kettenmann, H. and Steinhauser, C. 2015. Characterization of panglial gap junction networks in the thalamus, neocortex, and hippocampus reveals a unique population of glial cells. *Cerebral Cortex* 25 (10), pp. 3420-3433. 10.1093/cercor/bhu157

Publishers page: <http://dx.doi.org/10.1093/cercor/bhu157>

Please note:

Changes made as a result of publishing processes such as copy-editing, formatting and page numbers may not be reflected in this version. For the definitive version of this publication, please refer to the published source. You are advised to consult the publisher's version if you wish to cite this paper.

This version is being made available in accordance with publisher policies. See <http://orca.cf.ac.uk/policies.html> for usage policies. Copyright and moral rights for publications made available in ORCA are retained by the copyright holders.





**Characterization of panglial gap junction networks in the thalamus, neocortex and hippocampus reveals a unique population of glial cells**

Journal:	<i>Cerebral Cortex</i>
Manuscript ID:	CerCor-2014-00123.R1
Manuscript Type:	Original Articles
Date Submitted by the Author:	n/a
Complete List of Authors:	Griemsmann, Stephanie; University of Bonn, Institute of Cellular Neurosciences Höft, Simon; University of Bonn, Institute of Cellular Neurosciences Bedner, Peter; University of Bonn, Institute of Cellular Neurosciences Zhang, Jiong; University of Bonn, Institute of Cellular Neurosciences von Staden, Elena; University of Bonn, Institute of Cellular Neurosciences Beinhauser, Anna; University of Bonn, Institute of Cellular Neurosciences Degen, Joachim; University of Bonn, LIMES Institute, Molecular Genetics Dublin, Pavel; University of Bonn, Institute of Cellular Neurosciences Cope, David; Cardiff University, School of Biosciences Richter, Nadine; MDC for Molecular Medicine, Cellular Neuroscience Crunelli, Vincenzo; Cardiff University, School of Biosciences Jabs, Ronald; University of Bonn, Institute of Cellular Neurosciences Willecke, Klaus; University of Bonn, LIMES Institute, Molecular Genetics Theis, Martin; University of Bonn, Institute of Cellular Neurosciences Seifert, Gerald; University of Bonn, Institute of Cellular Neurosciences Kettenmann, Helmut; MDC for Molecular Medicine, Cellular Neuroscience Steinhauser, Christian; University of Bonn, Institute of Cellular Neurosciences
Keywords:	astrocytes, connexin, heterogeneity, oligodendrocytes, genetic deletion

**Characterization of panglial gap junction networks in the thalamus,  
neocortex and hippocampus reveals a unique population of glial cells**

Running title: Panglial networks in the thalamus, cortex and hippocampus

Stephanie Griemsmann<sup>a,1</sup>, Simon P.Höft<sup>a,1</sup>, Peter Bedner<sup>a</sup>, Jiong Zhang<sup>a</sup>, Elena von Staden<sup>a</sup>,  
Anna Beinhauer<sup>a</sup>, Joachim Degen<sup>b</sup>, Pavel Dublin<sup>a</sup>, David W. Cope<sup>c</sup>, Nadine Richter<sup>d</sup>,  
Vincenzo Crunelli<sup>c</sup>, Ronald Jabs<sup>a</sup>, Klaus Willecke<sup>b</sup>, Martin Theis<sup>a</sup>, Gerald Seifert<sup>a</sup>, Helmut  
Kettenmann<sup>d</sup>, Christian Steinhäuser<sup>a,2</sup>

<sup>a</sup>Institute of Cellular Neurosciences, Medical Faculty, University of Bonn, Sigmund Freud  
Str. 25, 53105 Bonn, Germany.

<sup>b</sup>Life and Medical Sciences (LIMES) Institute, Molecular Genetics, University of Bonn,  
53115 Bonn, Germany.

<sup>c</sup>School of Biosciences, Cardiff University, Cardiff CF10 3AX, UK.

<sup>d</sup>Max-Delbrück-Center for Molecular Medicine, Cellular Neuroscience, 13092 Berlin,  
Germany.

<sup>1</sup>These authors contributed equally to this work, <sup>2</sup>corresponding author

Running title: Panglial coupling in grey matter areas

Corresponding author: Christian Steinhäuser, PhD, University of Bonn, Institute of Cellular  
Neurosciences, Sigmund Freud Strasse 25, D-53105 Bonn Germany; Tel: +49 228 287 14669;  
Fax: +49 228 287 19121, email: christian.steinhaeuser@ukb.uni-bonn.de

Authors declare no competing financial interests.

1  
2  
3  
4  
5  
6  
7  
8  
9  
10  
11  
12  
13  
14  
15  
16  
17  
18  
19  
20  
21  
22  
23  
24  
25  
26  
27  
28  
29  
30  
31  
32  
33  
34  
35  
36  
37  
38  
39  
40  
41  
42  
43  
44  
45  
46  
47  
48  
49  
50  
51  
52  
53  
54  
55  
56  
57  
58  
59  
60

**Abstract**

The thalamus plays important roles as a relay station for sensory information in the CNS. Although thalamic glial cells participate in this activity, little is known about their properties. In this study we characterized the formation of coupled networks between astrocytes and oligodendrocytes in the murine ventrobasal thalamus and compared these properties with those in the hippocampus and cortex. Biocytin filling of individual astrocytes or oligodendrocytes revealed large panglial networks in all three grey matter regions. Combined analyses of mice with cell type-specific deletion of connexins, semi-quantitative RT-PCR and Western blotting showed that Cx30 is the dominant astrocytic connexin in the thalamus. Many thalamic astrocytes even lack expression of Cx43, while in the hippocampus astrocytic coupling is dominated by Cx43. Deletion of Cx30 and Cx47 led to complete loss of panglial coupling, which was restored when one allele of either connexins was present. Immunohistochemistry revealed a unique antigen profile of thalamic glia and identified an intermediate cell type expressing both Olig2 and Cx43. Our findings further the emerging concept of glial heterogeneity across brain regions.

**Key words**

Astrocytes, connexin, heterogeneity, genetic deletion, oligodendrocytes.

## Introduction

Gap junction channels are composed of connexin (Cx) proteins, which are differentially expressed between cell types, during development and across brain regions (Dermietzel et al. 1989; Kunzelmann et al. 1999; Nagy and Rash 2000; Schools et al. 2006; Giaume et al. 2010). Astrocytes express Cx43 (gene name, *Gja1*), Cx30 (*Gjb6*) and Cx26 (*Gjb2*), while oligodendrocytic gap junction channels are formed by Cx47 (encoded by the gene *Gjc2*) and Cx32 (encoded by *Gjb1*). In addition to inter-astrocytic (A:A) and inter-oligodendrocytic (O:O) coupling, recent evidence suggests that astrocytes and oligodendrocytes *in vivo* also form functional gap junction networks (GJNs) (A:O; pial coupling), both in white and grey matter (Maglione et al. 2010; Wasseff and Scherer 2011; Tress et al. 2012). Gap junctional communication between oligodendrocytes seems to be crucial for proper myelination and axonal survival (Nualart-Marti et al. 2013). Astrocytic GJNs fulfill a variety of important functions, including regulation of the K<sup>+</sup> and glutamate homeostasis and delivery of energy metabolites to sustain synaptic transmission (Pannasch et al. 2011; Wallraff et al. 2006; Rouach et al. 2008, reviewed by Theis and Giaume 2012; Pannasch and Rouach 2013). The molecular and functional data available as well as antibody staining (Nagy et al. 1997) led to the concept that Cx43 is abundantly expressed and present in all astrocytes throughout the brain.

However, so far the functional expression of connexins has only been analyzed in a few brain regions, e.g. the hippocampus, neocortex, cerebellum and corpus callosum. Despite the eminent function of the thalamus in processing sensory information and its involvement in sleep-related rhythms (Steriade 2006; Crunelli and Hughes 2010), little is known about the functional properties of glial cells in this area. In the ventrobasal thalamic nuclei, which receive sensory input from the vibrissae and project to the barrel cortex (Bokor et al. 2008; Bourassa et al. 1995), astrocytic Ca<sup>2+</sup> oscillations were reported to drive neuronal excitation. Moreover, long-term enhancement of astrocytic glutamate release was shown to be

dependent on the activation of metabotropic glutamate receptor and  $\text{Ca}^{2+}$  elevation in astrocytes (Parri et al. 2001;Pirttimaki et al. 2011;Pirttimaki et al. 2012). Here we set out to characterize glial gap junction coupling in these nuclei, combining tracer filling in mice with cell type specific deletion of connexins, sqRT-PCR and Western blotting. In addition, immunohistochemistry was applied to investigate the antigen profile of thalamic astrocytes. Our findings demonstrate that thalamic astrocytes display properties, which significantly differ from those seen in other brain regions and identify an intermediate cell type co-expressing astroglial and oligodendroglial proteins. This insight supports the emerging view that astrocytes *in vivo* comprise a heterogeneous cell population (Matyash and Kettenmann 2010;Zhang and Barres 2010) whose physiological significance still has to be defined.

**Materials and Methods**

*Animals*

Experiments were performed in C57Bl6J (Charles River, Wilmington, USA), Cx43kiECFP (Degen et al. 2012), Cx30kiLacZ (Teubner et al. 2003), Cx30kiLacZ; Cx47kiEGFP (Tress et al. 2012), hGFAP-EGFP (Nolte et al. 2001), PLP-GFP (Fuss et al. 2000), Cx30kiLacZ; Cx43fl/fl; hGFAP-Cre (Wallraff et al. 2006) and Cx26fl/fl; nestin-Cre mice (Nagy et al. 2011). Animals of either sex were investigated at postnatal day (p) 30-60 if not indicated otherwise. Mice were kept under standard housing conditions. All experiments were carried out in accordance with local, state and European regulations.

*Slice preparation*

Animals were anesthetized with Isoflurane (Abbott, Wiesbaden, Germany), killed by decapitation and the brains were quickly removed. The brains were placed in ice cold preparation solution containing (in mM): 87 NaCl, 2.5 KCl, 1.25  $\text{NaH}_2\text{PO}_4$ , 25  $\text{NaHCO}_3$ , 7  $\text{MgCl}_2$ , 0.5  $\text{CaCl}_2$ , 25 glucose, 75 sucrose and bubbled with carbogen (95%  $\text{O}_2$  / 5% $\text{CO}_2$ ). If



not stated otherwise chemicals were purchased from Sigma-Aldrich (Taufkirchen, Germany). Using a vibratome (VT1200S, Leica, Nussloch, Germany; HM650V, Microm International, Walldorf, Germany), horizontal and coronal slices containing the ventroposteromedial (VPM) and ventroposterolateral (VPL) nuclei of the thalamus, the hippocampus and cortex were obtained. Slice thickness was 200  $\mu\text{m}$ . Slices were stored at 35°C for 20 min, cooled down to room temperature and transferred into artificial cerebrospinal fluid (ACSF) containing (in mM): 126 NaCl, 3 KCl, 2  $\text{MgSO}_4$ , 2  $\text{CaCl}_2$ , 10 glucose 1.25  $\text{NaH}_2\text{PO}_4$  and 26  $\text{NaHCO}_3$  (room temperature). For some experiments slices were incubated in ACSF supplemented with 1  $\mu\text{M}$  sulforhodamine 101 (SR101; Molecular Probes, Life Technologies, Darmstadt, Germany) at 35°C for 20 min.

### *Electrophysiological recordings*

For recordings and tracer coupling experiments, slices were transferred to a recording chamber and continuously perfused with carbogenized ACSF. Cells were visualized using an upright microscope equipped with infrared DIC (Eclipse E600FN or Eclipse FN1, Nikon, Düsseldorf, Germany; Axioskop2, Zeiss, Jena, Germany) at 60-fold magnification. Whole-cell voltage clamp experiments were performed on cells identified by endogenous fluorescence or staining with the astrocyte marker SR101 (Kafitz et al. 2008; Nimmerjahn et al. 2004). Pipettes were fabricated from borosilicate glass (Science Products) and had a resistance of 2 to 6  $\text{M}\Omega$  when filled with internal solution containing (in mM): 130 K-gluconate, 1  $\text{MgCl}_2$ , 3  $\text{Na}_2\text{-ATP}$ , 20 HEPES, 10 EGTA, pH 7.2 supplemented with the tracer 0.5% N-biotinyl-L-lysine (biocytin, Sigma-Aldrich). Currents were recorded employing either an EPC-7, EPC-8, or EPC-10 patch clamp amplifier (Heka, Lambrecht, Germany) and monitored by TIDA software (Heka). Data were sampled at 6 to 30 kHz and filtered at 3 to 10 kHz. Input and series resistance were regularly checked by applying +10 mV pulses. The holding potential was -80 mV. Tracer filling was performed for 20 min, afterwards slices

were fixed in 4% paraformaldehyde (PFA) in 0.1 M phosphate buffered saline (PBS), pH 7.4 at 4°C.

*Immunohistochemistry*

Mice were anesthetized by intraperitoneal injection of 80 mg/kg Ketamine hydrochloride (Medistar, Ascheberg, Germany) and 1.2 mg/kg Medetomidine hydrochloride (cp pharma, Burgdorf, Germany) and transcardially perfused with PBS followed by 4% PFA. Brains were removed, postfixed and cut on a vibratome (VT1200S, Leica) into horizontal slices (40 µm) and stored in PBS at 4°C for subsequent staining. Slices were blocked for 2-4 h at room temperature in PBS containing 2% TritonX-100 and 10% normal goat serum (NGS; Millipore). The first antibodies were incubated in PBS containing 0.1% TritonX-100 and 2% NGS at 4°C overnight; rabbit-α-β-Gal (Molecular Probes, A11132) 1:400; mouse-α-GFP (Invitrogen, Life Technologies, Darmstadt, Germany, A11120) 1:500; rabbit-α-Olig2 (Millipore, Darmstadt, Germany; AB9610) 1:1000; mouse-α-GS (Millipore, MAB302) 1:200; rabbit-α-Iba1 (Wako, Neuss, Germany; 019-19741) 1:400; mouse-α-NeuN (Millipore, MAB377) 1:200; rabbit-α-NG2 (Millipore, AB 5320) 1:100; goat-α-GFP(FITC) (Abcam, Cambridge, UK; ab6662-100) 1:500; chicken-α-GFP 1:600 (Abcam; ab13970). The next day slices were washed three times in PBS and incubated with the corresponding secondary antibodies in the antibody solution for 1.5 h at room temperature; goat-α-mouseA647 1:500; goat-α-rabbitA647 1:500; donkey-α-rabbitA647 1:500; goat-α-rabbitAlexa594 1:500-1:800; goat-α-mouseAlexa488 1:600, goat-α-chickenAlexa488 1:500 (all antibodies from Invitrogen). Slices were washed three times and incubated with Hoechst (Molecular Probes) (1:100 in dH<sub>2</sub>O) or Draq5 (Biostatus, Shepshed, UK ) (1:1000 in PBS) for nuclei staining, washed again and mounted on coverslides with Aquapolymount (Polysciences Europe, Eppelheim, Germany).



Biocytin was visualized with Streptavidin-Cy3 (Sigma) 1:300, -Cy2 1:100 or -Cy5 (Jackson ImmunoResearch, Suffolk, UK) 1:200 applied in the staining protocol above. Additionally, for the immunohistochemical analysis of the biocytin injected cells 2-5% BSA was added to the blocking and antibody solutions, secondary antibodies were incubated for 2 h at room temperature. Images were acquired at a 1-2  $\mu\text{m}$  interval using a fluorescence microscope (Axiophot, Zeiss, Jena, Germany) employing MetaVue software, a confocal Leica TCS NT or a confocal Leica SPE microscope.

#### *Evaluation of reporter expression in acute brain slices*

Brains of adult Cx43<sup>ECFP/+</sup> and PLP-GFP mice were cut in 200  $\mu\text{m}$  thick slices. Stacks of optical sections were obtained with an SP5 LSM (Leica), equipped with an infrared ultra-short-pulse laser (MaiTai; Spectra Physics, Darmstadt, Germany). Two photon absorption was achieved by excitation of the fluorochromes with femtosecond pulses of infrared light with repetition rates of 80 MHz. The wavelength for dual excitation was adjusted for best signal to noise ratio: ECFP/SR101: 870-890 nm (1 W); GFP/SR101: 950 nm (0.5 W). Reflected and transmitted light was collected with two channel non-descanned detectors in each light pathway. For GFP/SR101 reflected emission light was separated with an FITC-TRITC filter cube (Leica). For ECFP/SR101 reflected light was splitted with an YFP-CFP filter cube (Leica) and the transmitted emission light was separated by a FITC-TRITC filter combination. Depending on the brain area, volumes of 455x455x40–200  $\mu\text{m}$  were scanned with a resolution of 1024x1024x80-400 pixels. Image analysis was performed with Leica LAS AF software.

#### *Semi-quantitative RT-PCR for examination of hippocampal and thalamic connexin levels*

C57/BL6J mice were anaesthetized and decapitated. Their brains were cut into 200  $\mu\text{m}$  thick slices in horizontal orientation as described above and the whole hippocampi and the

ventrobasal thalami were dissected. Total RNA was isolated from the tissue by Trizol (Life Technologies) and dissolved in DEPC-treated water (10 µl). Genomic DNA was removed by DNase treatment in a mixture containing PCR buffer, 2.5 mM MgCl<sub>2</sub>, 10 mM DTT (all Life Technologies), 20 U DNaseI (Roche, Mannheim, Germany) and 40 U RNase inhibitor (Promega, Mannheim, Germany; final volume 20 µl; incubation at 37°C for 30 min). Oligo (dT)25 linked Dynabeads™ (Life Technologies) were used to isolate mRNA. The mRNA was suspended in water (20 µl) and stored at -20°C.

Semiquantitative RT-PCR was performed as a single enzyme procedure using rTth DNA polymerase (TaqMan™ EZ RT-PCR Kit, Applied Biosystems, Darmstadt, Germany). The final reaction volume was 12.5 µl containing 1 µl mRNA, TaqMan™ EZ buffer, 3x300 µM dNTPs (dATP, dCTP, dGTP), 600 µM dUTP, 3 mM Mn(OAc)<sub>2</sub>, 1.25 U rTth DNA polymerase, 0.125 U uracil-N-glycosylase, 100 nM fluorogenic TaqMan™ probe and 600 nM of *Gja1* and *Gjb6* primers, respectively (Table 1). For β-actin quantification, a Taqman probe/primer mix was used (Applied Biosystems). RT-PCRs for *Gja1*, *Gjb6* and β-actin were run in parallel tubes for each sample. Samples were incubated at 50°C (2 min), and first strand synthesis was performed at 60°C (20 min). After denaturation (95°C, 5 min), 40 cycles were performed (denaturation at 94°C, 15 s; primer annealing and extension at 59°C, 60 s). Fluorescence intensity was readout during each annealing/extension step. *Data Analysis:* We determined the expression ratio of *Gja1*/β-actin and *Gjb6*/β-actin genes by comparing threshold cycle (C<sub>T</sub>) values of the target gene with those of the reference gene at the same fluorescence emission Rn. The respective amplification efficiencies were determined by the serial dilution method (Seifert et al., 2009).

*Western blot analysis*

Brain tissue of hippocampus and thalamus from C57/BL6J mice were lyzed in modified RIPA lysis buffer (50 mM Tris, 150 mM NaCl, 0.5% Nonidet P40, 0.5% Na-DOC, 1% Triton X-

100, PH 7.5) supplemented with protease and phosphatase inhibitor single-use cocktail (Thermo Scientific, St. Leon-Rot, Germany; 78443). The tissue samples were homogenized and incubated on ice for 30 min. Samples were centrifuged for 30 min at 13,000x g at 4°C and the supernatants were transferred into new tubes. Total protein content was assayed with BCA (Pierce, Bonn, Germany) and 30-50 µg of total protein per lane was used. Lysates were mixed with sample buffer (62.5 mM Tris-Cl, pH 6.8, 3% SDS, 0.01% bromophenol blue, 5% b-mercaptoethanol, 10% glycerol) and heat-incubated for 10 min at 65°C before they were shortly centrifuged at 4°C. Proteins were separated with standard 10-12% SDS-PAGE under denaturing conditions and electroblotted onto a PVDF membrane. Membranes were blocked with 5% milk powder in TBS (pH 7.4) containing 0.05% Tween-20 and incubated over-night at 4°C on a rotator with the following primary antibody solutions: rabbit-anti-Cx43 (1:5000; Sigma), rabbit-anti-Cx30 (Zymed-Invitrogen, Life Technologies) 1:250, mouse-anti- $\alpha$ -tubulin (Sigma) 1:20,000. Secondary antibodies used: goat-anti-mouse HRP conjugate (GE healthcare, München, Germany) 1:10,000, goat-anti-rabbit HRP conjugate (GE healthcare) 1:10,000. All antibodies, including secondary antibodies were diluted in 5% milk powder in TBS (pH 7.4) containing 0.05% Tween-20. HRP was visualized with the West Dura substrate (Pierce) and chemiluminescence was detected with the Gene Gnome digital documentation system (Synoptics, Cambridge, UK). Raw data analysis and densitometry were performed with GeneTools quantification software (Synoptics). Cx43 and Cx30 were always measured from the same samples.

#### *Data analysis:*

Data are given as mean  $\pm$  SEM. Differences between data were tested for significance using Student's t-test, Mann-Whitney U-test or ANOVA followed by Tukey's test, as appropriate. Differences between means were regarded as significant at  $p < 0.05$  (\*) or  $p < 0.01$  (\*\*).

**Results**

Gap junction coupling is a hallmark of glial cells and plays an important role in brain function, albeit these networks have been characterized only in a few regions yet. Here we employed mouse lines with fluorescently labelled astrocytes and oligodendrocytes to investigate coupling between glial cells in the ventrobasal thalamus (VPL/VPM nuclei) in comparison to neocortex and the stratum radiatum (s.r.) of the hippocampal CA1 region.

**Thalamic glial cells are abundantly coupled**

Astrocytes were identified by their passive current pattern, typical morphology and bright EGFP fluorescence in hGFAP-EGFP mice (Fig. 1 A<sub>1</sub>) (Nolte et al. 2001; Matthias et al. 2003). Biocytin injection into a thalamic astrocyte revealed large networks of cells, which did not further increase beyond the first two postnatal weeks (p9-11,  $84 \pm 13$  cells; p13-15,  $111 \pm 8$  cells; p30-60,  $108 \pm 11$  cells; p90-120,  $95 \pm 8$  cells; Fig. 1C). The ventrobasal thalamus, particularly the VPL, contains densely packed myelinated fiber tracts. Unexpectedly, in several cases we observed spread of the tracer from the astrocyte into the myelin sheath along the fiber tracts (Fig. 1A<sub>2</sub>, B, see inset in B). Orientation of GJNs along functional entities has been observed previously in the barrel cortex (Houades et al. 2008) and in the olfactory bulb (Roux et al. 2011).

**Comparative analyses of GJNs in the thalamus, neocortex and hippocampus reveal distinct expression of Cx43 and Cx30**

Earlier studies have demonstrated a major impact of Cx43 on the size of GJNs in the hippocampus (Wallraff et al. 2006; Gosejacob et al. 2011). To compare the relevance of Cx43 in thalamic, hippocampal and cortical astrocytes, tracer coupling was investigated in heterozygous Cx43<sup>ki</sup>ECFP mice, in which one allele of *Gjal* was replaced by ECFP (p30-64; Fig. 2A-C). In these mice, ECFP is expressed by astrocytes but not by NG2 cells (Degen et al.

2012). In wild type littermates, biocytin spread to about 80 coupled cells, irrespective of the brain region investigated (Fig. 2D<sub>1</sub>). Knockout of one *Cx43* allele in Cx43kiECFP mice led to a significant decrease in the number of coupled cells in the hippocampus (*Gjal*<sup>+/+</sup>, 79 ± 9 cells; *Gjal*<sup>ECFP/+</sup> 51 ± 10 cells), while in the somatosensory cortex and thalamus no changes in network size were observed (cortex, *Gjal*<sup>+/+</sup>, 75 ± 9 cells; *Gjal*<sup>ECFP/+</sup>, 71 ± 9 cells; thalamus, *Gjal*<sup>+/+</sup>, 79 ± 4 cells; *Gjal*<sup>ECFP/+</sup>, 87 ± 10 cells) (Fig. 2D<sub>1</sub>). Consistently, in these heterozygous Cx43-ECFP mice a vast majority of the biocytin-labelled cells in the hippocampus expressed Cx43, as indicated by expression of the reporter gene ECFP. In contrast, only part of the coupled cells in the thalamus was ECFP<sup>+</sup> and the number of ECFP<sup>+</sup> cells within cortical GJNs was also lower than in the hippocampus (Fig. 2D<sub>2</sub>). We compared the expression of *Gjal* and *Gjb6* in the thalamus and the hippocampus at the transcript level. As expected, sqRT-PCR revealed a lower *Gjal*/β-actin mRNA ratio in the thalamus (0.09 ± 0.03) vs. hippocampus (0.12 ± 0.02). Notably, the *Gjb6*/β-actin mRNA ratio was higher in the thalamus (0.09±0.02) vs. hippocampus (0.06 ± 0.01) (Fig 2E). Our data confirm earlier studies showing that Cx43 is predominantly expressed in hippocampal and cortical GJNs. This is in contrast to the thalamus where the majority of coupled cells lack Cx43.

### Many thalamic astrocytes are devoid of Cx43

The surprising finding that a majority of coupled cells in the thalamus lacked Cx43-ECFP raised the question of their identity. To address this issue, we assessed the proportion of ECFP<sup>+</sup> cells among thalamic astrocytes employing SR101 (Kafitz et al. 2008; Nimmerjahn et al. 2004) and two-photon laser scanning microscopy in acute slices. Indeed, 50% of the SR101<sup>+</sup> cells lacked ECFP (Fig. 3A). This clearly differed from the hippocampus where the vast majority of SR101<sup>+</sup> cells also expressed ECFP (Fig. 3B). To ensure that our data were not distorted through potential SR101 labeling of oligodendrocytes (Wasseff and Scherer 2011), transgenic mice with fluorescence labeling of oligodendrocytes (PLP-GFP mice) (Fuss

et al. 2000) were employed. In both brain regions only a few, weakly SR101<sup>+</sup> cells were also GFP<sup>+</sup> (thalamus, 1.9 ± 0.5%; hippocampus, 1 ± 0.8%) (Fig. 3C, D). Since these weakly SR101<sup>+</sup>/GFP<sup>+</sup> cells were not visible with conventional epifluorescence microscopy used at the patch clamp setups, SR101 was a reliable marker to identify astrocytes. These findings were in line with the assumption that a significant proportion of the thalamic astrocytes lack Cx43.

**Thalamic GJNs are mainly formed by Cx30**

The moderate participation of Cx43-ECFP<sup>+</sup> cells in the GJNs and our transcript analysis (Fig. 2) suggested that astrocytic coupling in the thalamus was dominated by Cx30. To investigate the impact of this isoform on thalamic coupling we employed homozygous Cx30kiLacZ mice, in which the coding region of the *Gjb6* gene was replaced by the reporter gene LacZ (Teubner et al. 2003). In these mice biocytin filling of SR101<sup>+</sup> thalamic astrocytes showed a drastic decrease in coupling compared to littermate controls (*Gjb6*<sup>+/+</sup>, 81 ± 6 cells; *Gjb6*<sup>LacZ/LacZ</sup>, 22 ± 3 cells) (Fig. 4A), and even complete uncoupling in some cases (n = 5; not shown). These findings differed significantly from the hippocampus, where loss of Cx30 decreased coupling only by 22% (Gosejacob et al. 2011). SR101 uptake did not influence tracer coupling in the thalamus (SR101 incubation, 113 ± 8 cells, n = 12; control, 106 ± 12 cells, n = 8, not shown). Further experiments performed in mice deficient for Cx30 and Cx 43 (*Gjb6*<sup>LacZ/LacZ</sup>; *Gjal*<sup>fl/fl</sup>; *hGFAP-Cre*) revealed complete disruption of gap junctional communication in 16 out of 18 biocytin-filled thalamic SR101<sup>+</sup> cells. Residual coupling (8 ± 6 cells) was observed in two cases (not shown). Since Cx26 was reported to be abundantly expressed in the thalamus (Nagy et al. 2011), we examined the potential contribution of Cx26 to GJN in the thalamus in mice devoid of Cx26 (*Gjb2*<sup>fl/fl</sup>; *nestin-Cre*). Analysis of biocytin transfer in the hippocampus and thalamus revealed no significant difference between control and Cx26 knockout mice (thalamus, control, 150 ± 23 cells, n = 9; *Gjb2*<sup>fl/fl</sup>; *nestin-Cre*, 112 ± 17 cells, n = 11; hippocampus, control, 91 ± 9 cells, n = 8; *Gjb2*<sup>fl/fl</sup>; *nestin-Cre*, 118 ± 14 cells, n = 9, not



shown). Accordingly, Cx26 does not seem to significantly contribute to functional GJ channels in the brain areas analyzed.

To further investigate connexin expression on a cellular level we performed reporter gene analysis in *Gjal*<sup>ECFP/+</sup>; *Gjb6*<sup>LacZ/+</sup> mice. Since LacZ is not expressed in the hippocampus of these mice (Gosejacob et al. 2011), experiments were restricted to the thalamus (Fig. 4B). Quantification of the overlap of ECFP and  $\beta$ -Gal signal unveiled that almost all ( $43,051 \pm 1,627$   $\beta$ -Gal<sup>+</sup> cells/mm<sup>3</sup> of  $43,719 \pm 1,457$  total cells/mm<sup>3</sup>) of the thalamic astrocytes express Cx30, and many of them lack Cx43 ( $8,904 \pm 1,117$   $\beta$ -Gal<sup>+</sup>/ECFP<sup>-</sup> cells/mm<sup>3</sup>) (Fig. 4B<sub>4</sub>). The latter population probably accounts for the uncoupled cells found in the thalamus of Cx30 knockout (*Gjb6*<sup>LacZ/LacZ</sup>) mice (cf. above).

Western blot analysis revealed an up-regulation of connexin expression during postnatal development (Fig. 4C, D). In the hippocampus Cx30 and Cx43 increased twofold between p14 and p53, while Cx30 protein levels increased more than threefold during this period in the thalamus. Thus, in the adult brain, thalamic Cx30 levels significantly exceed those in the hippocampus, while Cx43 protein content does not differ (Fig. 4C<sub>2</sub>, D<sub>2</sub>). In conclusion, astrocytic coupling in the adult thalamus is mediated predominantly by Cx30.

### **Oligodendrocytes and astrocytes form functional panglial networks**

The experiments so far documented a population of astrocytes in the thalamus lacking Cx43, but abundantly expressing Cx30. Further characterization of cell identity in GJNs was carried out employing hGFAP-EGFP mice. Notably, EGFP was abundantly expressed in both thalamus and hippocampus, although GFAP antibody staining in the thalamus labels only very few cells (not shown; see Parri and Crunelli 2002; Frassoni et al. 2000). Thus, glutamine synthetase (GS) was used as a marker for astrocytes (Coulter and Eid 2012; Norenberg 1979; Sonnewald et al. 1997). GS was expressed by less than half of the biocytin-coupled cells in the thalamus ( $49 \pm 8$  of  $100 \pm 13$  cells) while most of the coupled cells in the hippocampal

CA1 region were  $GS^{+}$  ( $106 \pm 10$  of  $129 \pm 11$  cells) (Fig. 5A, B). Surprisingly, when staining against Olig2, a transcription factor expressed in cells of the oligodendrocyte lineage (Trotter et al. 2010; Marshall et al. 2005; Nishiyama et al. 2009) we found abundant expression in thalamic and cortical networks ( $49 \pm 8$  of  $75 \pm 7$  cells and  $62 \pm 24$  of  $102 \pm 25$  cells, respectively; Fig. 5C-E). In hippocampal GJNs Olig2 labeling was much less prevalent ( $19 \pm 4$  of  $129 \pm 18$  cells) (Fig. 5C, D). The data indicated participation of oligodendrocytes in GJNs of the three brain regions investigated. Furthermore in the hippocampus, GS and Olig2 label distinct cell populations while the overlap in staining as derived from cell counting (Fig. 5A4, C4) indicated that in the thalamus these markers are not cell type-specific.

In contrast to recent findings in the corpus callosum (Maglione et al. 2010), we never observed  $NG2^{+}$  cells within thalamic, hippocampal or cortical GJNs (thalamus, 0 of  $117 \pm 11$  cells,  $n = 8$ ; hippocampus, 0 of  $136 \pm 18$  cells,  $n = 8$ ; cortex, 0 of  $143 \pm 14$  cells,  $n = 6$ ).

Moreover  $Iba1^{+}$  microglia (thalamus  $n = 9$ , hippocampus  $n = 8$ ) or  $NeuN^{+}$  neurons (thalamus  $n = 9$ , hippocampus  $n = 6$ ) never participated in the networks (not shown).

The abundance of  $Olig2^{+}$  cells in thalamic GJNs challenged the concept of pure astrocytic networks. Astrocytic connexins form heterotopic channels with oligodendrocytic connexins *in vitro* (Orthmann-Murphy et al. 2007; Magnotti et al. 2011), and recently functional panglial networks have also been observed *in situ* (Maglione et al. 2010; Wasseff and Scherer 2011; Tress et al. 2012). To confirm putative astrocyte-oligodendrocyte coupling, PLP-GFP<sup>+</sup> oligodendrocytes or SR101<sup>+</sup> astrocytes were patched and tracer spread was quantified. Filling of astrocytes with biocytin in the thalamus und hippocampus revealed abundant coupling (thalamus,  $118 \pm 15$ ; hippocampus,  $133 \pm 16$ ; Fig. 6A, C, E<sub>1</sub>). Notably, the GJNs were not significantly smaller when filling oligodendrocytes with the tracer (thalamus,  $87 \pm 14$ ; hippocampus,  $82 \pm 15$ ), and coupling did also not differ between brain regions (Fig. 6B, D, E<sub>1</sub>). In a next step we analyzed the proportion of PLP-GFP<sup>+</sup> cells in these GJNs and found considerable differences between brain regions. In the thalamus more than 50% of biocytin

labelled cells were GFP<sup>+</sup>, while in the hippocampus less than 14% were GFP<sup>+</sup>. However, in a given brain region, the proportion of GFP<sup>+</sup> cells was the same when injecting an astrocyte or an oligodendrocyte (Fig. 6E<sub>2</sub>). Thus, tracer spread into the panglial syncytium was independent of the type of glia initially patched. The diverging contribution of PLP-GFP<sup>+</sup> cells to the GJNs in the two brain regions obviously reflects the different densities of the PLP-GFP<sup>+</sup> cells (Fig. 3C, D; Fig. 6). Additionally, panglial coupling was investigated prior to the expected onset of Cx30 protein expression (Kunzelmann et al., 1999). Biocytin injection in astrocytes of p9-11 old PLP-GFP mice revealed abundant panglial coupling ( $87 \pm 18$  coupled cells; among them 34% GFP<sup>+</sup> cells;  $n = 14$ ; Suppl. Fig. 1). These data directly demonstrate that both in the hippocampus and thalamus, astrocytes and oligodendrocytes form panglial GJNs.

### **Panglial coupling in the thalamus and hippocampus is mainly mediated by heterotypic channels containing Cx30**

To investigate the molecular basis of panglial coupling in the thalamus and hippocampus we employed knockout mice in which *Gjb6* was replaced by LacZ and *Gjc2* by EGFP (Tress et al. 2012). Cx30 and Cx47 form functional gap junction channels with Cx32 and Cx43 respectively, thus mediating astrocyte to oligodendrocyte coupling (Orthmann-Murphy et al. 2007; Theis and Giaume 2012). Coupling analysis was performed by injecting biocytin in astrocytes from *Gjb6*<sup>+/LacZ</sup>; *Gjc2*<sup>EGFP/EGFP</sup> (Fig. 7A<sub>1</sub>), *Gjb6*<sup>LacZ/LacZ</sup>; *Gjc2*<sup>EGFP/EGFP</sup> (Fig. 7A<sub>2</sub>) and *Gjb6*<sup>LacZ/LacZ</sup>; *Gjc2*<sup>+/EGFP</sup> mice. In *Gjb6*<sup>LacZ/LacZ</sup>; *Gjc2*<sup>EGFP/EGFP</sup> mice, many of the biocytin-filled cells lacked coupling (thalamus, 43%; hippocampus, 60%; Fig. 7B), with the remaining cells showing only tiny networks (thalamus,  $5 \pm 1$ ; hippocampus,  $5 \pm 2$  coupled cells; Fig. 7C). Deletion of both Cx47 alleles and one *Gjb6* allele still resulted in large GJNs (thalamus,  $166 \pm 16$ ; hippocampus,  $79 \pm 14$  coupled cells; Fig. 7C), whereas only small GJNs were observed in *Gjb6*<sup>LacZ/LacZ</sup>; *Gjc2*<sup>+/EGFP</sup> mice (thalamus,  $28 \pm 11$ ; hippocampus,  $39 \pm 19$  coupled

cells). The proportion of oligodendrocytes within the GJNs, as assessed by Cx47-EGFP-fluorescence, varied considerably between the different genotypes (Fig. 7D). The tiny networks in mice lacking both Cx30 and Cx47 did not contain oligodendrocytes, while panglial networks were observed in thalamus and hippocampus of *Gjb6*<sup>+/-LacZ</sup>; *Gjc2*<sup>EGFP/EGFP</sup> and *Gjb6*<sup>LacZ/LacZ</sup>; *Gjc2*<sup>+/-EGFP</sup> mice. So far, functional channels formed by Cx47 and Cx30 have not been observed *in vivo*. Accordingly, our results suggest that in the thalamus astrocyte-to-oligodendrocyte coupling is mediated predominantly by heterotypic Cx30:Cx32 channels, while Cx43:Cx47 channels play a minor role.

**Glial cells in the thalamus express unusual antigen profiles**

As quantification indicated overlap of GS and Olig2 immunoreactivity in the thalamic networks (Fig. 5), we addressed the question of antigen profiles employing reporter mice. Slices from Cx43<sup>ECFP/+</sup> mice were stained against Olig2. About half of the Cx43-ECFP<sup>+</sup> cells in the thalamus co-expressed Olig2 (20,267 ± 2,917 cells/mm<sup>3</sup> from a total of 38,563 ± 1,723 ECFP<sup>+</sup> cells/mm<sup>3</sup>) (Fig. 8A), while hippocampal ECFP<sup>+</sup> cells typically lacked Olig2 (3,155 ± 1,107 ECFP<sup>+</sup>/Olig2<sup>+</sup> cells/mm<sup>3</sup> from a total of 52,217 ± 3,215 ECFP<sup>+</sup> cells/mm<sup>3</sup>) (Fig. 8B). In the neocortex 20% of the ECFP<sup>+</sup> cells expressed Olig2 (3,240 ± 879 ECFP<sup>+</sup>/Olig2<sup>+</sup> cells/mm<sup>3</sup> from a total of 15,305 ± 1,126 ECFP<sup>+</sup> cells/mm<sup>3</sup>). These data indicate the existence of an ‘intermediate’ glial cell type in the thalamus and cortex that co-expressed astrocytic (*Gjal*) and oligodendrocytic (*Olig2*) genes. These cells proved to be mature astrocytes integrated in biocytin-labelled networks because co-immunostainig after biocytin injection revealed that in the thalamus 14% of the total number of coupled cells co-expressed of ECFP and Olig2 (58 ± 6 coupled cells, n=10 slices, Suppl. Fig. 2). Brain slices from PLP-GFP mice were stained against NG2 (Trotter et al. 2010), which revealed co-expression of NG2 and GFP in the hippocampus (17.9 % from a total of 26,447 ± 1,434 GFP<sup>+</sup> cells/mm<sup>3</sup>, n = 9 slices from 3 mice) while PLP-GFP<sup>+</sup> cells in the thalamus were not NG2<sup>+</sup> (0.2 % from 158,844 ± 4,092

GFP<sup>+</sup> cells/mm<sup>3</sup>, n = 9 slices from 3 mice, not shown). We noted that NG2<sup>+</sup> cells were very weakly PLP-GFP<sup>+</sup>. S100 $\beta$  is considered an astrocyte-specific marker in the hippocampus (Ogata and Kosaka 2002) and thalamus (Parri et al. 2010). In line with these previous findings, we detected only minor expression of S100 $\beta$  in PLP-GFP<sup>+</sup> oligodendrocytes (thalamus, 17.5 %; hippocampus, 18.1 %). Very few PLP-GFP<sup>+</sup> cells in the hippocampus co-expressed NG2 and S100 $\beta$  (1.6 %) while triple labeling was not observed in the thalamus. Almost all PLP-GFP<sup>+</sup> cells in the thalamus expressed GS (94.5 % from a total of 136,911  $\pm$  9,363 GFP<sup>+</sup> cells/mm<sup>3</sup>). In the hippocampus, GS immunoreactivity was mainly confined to astrocytes and only some GFP<sup>+</sup>/GS<sup>+</sup> cells could be detected (17.8 % from a total of 22,644  $\pm$  1,573 GFP<sup>+</sup> cells/mm<sup>3</sup>; n = 9 slices from 3 mice, data not shown).

In another study we used the astrocyte marker 10-formyltetrahydrofolate dehydrogenase (Aldh1L1), which revealed abundant Aldh1L1 labelling. Taking advantage of the PLP-GFP mouse line we found extensive overlap of Aldh1L1 staining and PLP-GFP (52% overlap from a total of 65,422  $\pm$  6,242 cells/mm<sup>3</sup>; n = 9 slices from 3 mice, Suppl. Fig. 3). Almost all of these cells were also positive for the oligodendrocyte marker Olig2 (97%). Furthermore, we observed Aldh1L1 labelled cells that co-expressed Olig2 (25%). Accordingly, classical cell type markers display an overlapping expression profile in the thalamus, but barely in the hippocampus.

## Discussion

Astrocytes form extensive GJNs, which are crucial for information processing (Pannasch and Rouach 2013), but such networks were only analyzed in a few brain areas. Since astrocyte properties may vary across CNS regions (Matyash and Kettenmann 2010; Zhang and Barres 2010), it is mandatory to extend investigation towards so far unexplored brain regions. Here, we provide the first detailed characterization of gap junction coupling in the ventrobasal

thalamus and report that thalamic glial cells possess properties that are clearly distinct from those in the hippocampus or neocortex.

Our findings challenge the general assumption that Cx43 is present in all astrocytes of the brain (Nagy et al. 1997; Pannasch and Rouach 2013). First, employing Cx43kiECFP mice (Degen et al. 2012), we found that genetic deletion of one allele of Cx43 decreased coupling in the hippocampus, but not in the thalamus and cortex. Transcript and protein analyses confirmed that Cx43 is less prevalent in the thalamus. Second, 25% of SR101<sup>+</sup> astrocytes in the thalamus of Cx30 ko mice were completely uncoupled. Third, SR101 staining (Nimmerjahn et al. 2004; Kafitz et al. 2008) of acute slices from Cx43kiECFP mice revealed that many SR101<sup>+</sup> astrocytes in the thalamus lack Cx43 promoter activity. By contrast, in the hippocampus almost all SR101<sup>+</sup> astrocytes were Cx43-ECFP<sup>+</sup> (Fig. 3B and Degen et al. 2012). Since SR101 did not significantly co-localize with PLP-GFP, we concluded that SR101 identifies astrocytes in the thalamus. Fourth, analysis of *Gjal*<sup>ECFP/+</sup>; *Gjb6*<sup>LacZ/+</sup> mice confirmed that a significant proportion of thalamic astrocytes lack Cx43. The higher proportion of Cx43-lacking astrocytes in the SR101 labeling experiment (about 50%, Fig. 3A) compared with  $\beta$ -Gal/ECFP staining (20%, Fig. 4B) might reflect that in the latter approach ECFP detection was improved by post fixation GFP antibody staining, while in SR101 labelled slices ECFP fluorescence was directly detected. Moreover,  $\beta$ -Gal staining might not detect all Cx30-expressing astrocytes (Gosejacob et al. 2011). Despite these methodical limitations, our results clearly demonstrate that astrocytic coupling in the thalamus is mainly based on Cx30 and that a significant subpopulation of thalamic astrocytes lack Cx43.

A previous study, using Lucifer yellow as a tracer, found no astrocyte coupling in the ventrobasal thalamus (Parri et al. 2001). Although all glial connexins are permeable for small molecules, permeability varies between subtypes (Elfgang et al. 1995). While the positively charged neurobiotin, which is structurally close to biocytin used here, permeates through Cx30 gap junction channels, the anionic tracer Lucifer yellow does not (Yum et al. 2007).



Thus, Parri et al. (2001) indirectly confirmed the predominant role of Cx30 in thalamic gap junction coupling described in the present study.

Immunostaining revealed abundant expression of Cx26 in the thalamus (Nagy et al. 2001; Nagy et al. 2011) although its functional impact remained unclear yet. We addressed this question by investigating coupling in Cx26 knockout mice, and our data do not indicate that this connexin significantly contributes to the GJNs. A similar conclusion can be drawn from analyses of astrocytes in mice devoid of Cx43 and Cx30, which produces uncoupling in the thalamus (this study) and hippocampus (Wallraff et al., 2006). The residual coupling we have observed in two astrocytes lacking Cx30 and Cx43 might reflect inefficient Cre recombination (Requardt et al. 2008). Whether Cx26 forms hemichannels or intracellular gap junctions still needs to be investigated.

So far, panglial coupling between astrocytes and oligodendrocytes *in situ* has only been detected in white matter tracts of corpus callosum and cerebellum (Maglione et al. 2010; Tress et al. 2012) while observations in neocortex were contradictory (Wasseff and Scherer 2011; Houades et al., 2008). We report abundant coupling between astrocytes and oligodendrocytes in the thalamus, hippocampus and neocortex. Panglial coupling was observed by immunostaining of Olig2 in biocytin filled networks and confirmed by tracer injections into PLP-GFP<sup>+</sup> cells. Notably, utilizing PLP-GFP mice we could demonstrate that more than half of the cells in thalamic GJNs were oligodendrocytes, irrespective of whether initially an astrocyte or oligodendrocyte was filled with biocytin. In the hippocampus, the size of GJNs was also independent of whether the tracer was injected into an astrocyte or oligodendrocyte, although the contribution of the latter was less than 15% due to the low number of PLP-GFP<sup>+</sup> cells in that region. Coupling was always bidirectional, as the extent of coupling and relative contribution of cell types to the GJNs was similar and independent of the initially injected cell type. We often observed that upon biocytin injection into astrocytes, tracer molecules spread along myelinated fiber tracts.

Gap junctions between astrocytes and oligodendrocytes are made by heterotypic channels between Cx43 (A) and Cx47 (O), or between Cx30 (A) and Cx32 (O) (Orthmann-Murphy et al. 2007). Cx47 function is directly dependent on Cx43 as the former decreases after conditional ko of Cx43 (May et al. 2013). Mutations in the Cx47 gene lead to reduced expression of myelin basic protein, astrogliosis and activation of microglia in mice (Tress et al. 2011) and Pelizaeus-Merzbacher-like disease in man (Uhlenberg et al. 2004). Genetic ablation of *Gjb6* and *Gjc2* in mice results in early onset of myelin pathology accompanied by severe motor impairments and partial premature death. In these mice complete loss of panglial networks in white matter tracts of cerebellum and corpus callosum was observed, while total network size was maintained indicating that O:O coupling was preserved (Tress et al. 2012). Whereas in the latter study oligodendrocytes were filled with the tracer, we were interested in astrocyte coupling. We observed that the thalamus of Cx30/Cx47 deficient mice was not only devoid of A:O coupling, but also almost completely lost inter-astrocytic coupling. This was unexpected, as Cx43-mediated A:A coupling should have been preserved under these conditions. Interestingly, one allele of *Gjc2* was sufficient to partially restore GJNs, including panglial coupling. Thus, Cx43 expression might not only stabilize Cx47 at the oligodendrocytic surface (May et al. 2013), but in turn affects Cx43 localization. Indeed, it has been demonstrated that ko of Cx47 leads to redistribution of astrocytic Cx43 away from the oligodendrocyte plasma membrane (Li et al. 2008). Alternatively, taking into account the relatively low incidence of Cx43 in that brain region, our data might indicate that thalamic astrocytes do not form homotypic Cx43 channels. Panglial coupling in the neocortex is also mediated by Cx47, while in white matter it is still under discussion whether A:O channels are formed by Cx47 or Cx32 (Wasseff and Scherer 2011; Maglione et al. 2010). In contrast to the corpus callosum (Maglione 2010), NG2 cells in the hippocampus, thalamus and neocortex were not part of the networks.

Since GFAP is rarely expressed in thalamic astrocytes (Frassoni et al. 2000) we considered GS and Aldh1L1 as a putative astrocytic marker. As expected from the literature (Norenberg 1979; Derouiche and Frotscher 1991), we found that hippocampal GJNs mostly comprised GS<sup>+</sup> cells. In clear contrast, in the thalamus only a minor fraction of coupled cells stained for GS, and many of them resembled oligodendrocytes in morphology. The hypothesis that thalamic oligodendrocytes abundantly express GS was confirmed by demonstrating that almost all PLP-GFP<sup>+</sup> cells expressed this enzyme. Accordingly, GS is not a reliable astrocyte marker in the thalamus (see also Cammer 1990; D'Amelio et al. 1990; Takasaki et al. 2010; Miyake and Kitamura 1992). Similarly, in the thalamus Aldh1L1 co-localized with PLP and Olig2, which confirms the existence of an intermediate glial phenotype.

Based on the assumption that Cx43 expression in the brain is confined to astrocytes, we have recently generated a Cx43<sup>ki</sup>ECFP mouse line and shown that in the hippocampus ECFP<sup>+</sup> cells express GFAP but not markers for neurons, NG2 cells or microglia (Degen et al., 2012).

Unexpectedly, here we found that Cx43-ECFP<sup>+</sup> cells in the adult thalamus and neocortex frequently express the basic helix-loop-helix transcription factor Olig2, which is considered a marker of oligodendrocytes (Trotter et al. 2010). Existence of such an intermediate glial cell type was also in line with our coupling analysis because upon biocytin injection into astrocytes, the proportion of Olig2<sup>+</sup> cells in the networks (Fig. 5C) exceeded the fraction of PLP-GFP<sup>+</sup> oligodendrocytes (Fig. 6E<sub>2</sub>) by about 10%. Furthermore we observed ECFP<sup>+</sup> and Olig2<sup>+</sup> cells in biocytin labelled networks. During cortical development, Olig2 is transiently expressed in astrocytes at embryonic stages and downregulated later on. Ablation of Olig2 in astrocytes leads to a reduction in the number of astrocytes in white matter of cortex and spinal cord and to unusual, sustained expression of GFAP in cortical grey matter astrocytes (Cai et al. 2007). Fate mapping of Olig2<sup>+</sup> cells in the diencephalon revealed pronounced gliogenesis of both oligodendrocytes and astrocytes in the ventral thalamus (Ono et al. 2008).

Collectively, our data suggest that in addition to *bona fide* astrocytes and oligodendrocytes, a

subpopulation of glial cells in the adult thalamus have a unique, intermediate phenotype, which emphasizes the heterogeneous nature of these cells.

Tight and intimate contact and signal interaction of myelinating cells, their precursors and their enwrapped axons is necessary for the integrity of axons both in the CNS and PNS (Nave 2010). Oligodendrocytes support axon function by transport of metabolites (Funfschilling et al. 2012; Lee et al. 2012). Because astrocytes also supply neurons with lactate in an activity-dependent manner (Pellerin and Magistretti 2012; Suzuki et al. 2011), the question arises whether lactate supply by astrocytes and oligodendrocytes is organized through parallel pathways or if panglial coupling is necessary for metabolic support of neurons and its axons. Mice lacking both oligodendrocytic connexins, Cx32 and Cx47 show thinner and vacuolated myelin sheets and axonal degeneration (Odermatt et al. 2003; Menichella et al. 2003), which is in line with the hypothesis that panglial GJNs are crucial for nutritional supply, e.g. glucose transport from blood vessels via astrocytes to oligodendrocytes and subsequent lactate transport into axons (Funfschilling et al. 2012). While previous work implied that metabolic supply of neurons only require A:A networks (Rouach et al. 2008), our data demonstrate that even in the hippocampus oligodendrocytes are part of the GJNs. Further experiments are needed to define the physiological impact of panglial coupling.

**Funding**

This work was supported by grants of the German Research Foundation (Wi 270/29-1 and 31-1, SFB 645, B2 to KW, SFB/TR3, C1 and STE 552/4 to CS, SFB/TR3, N01 and C9 to MT, KE 329/28 to HK); the Wellcome Trust (71436 to VC); and of the European Community (FP7-202167 NeuroGlia to CS, MT and VC). DWC was a Fellow of Epilepsy Research UK (P0802).

**Acknowledgements**

We thank Ina Fiedler, Anja Matijevic, Lukas Kunz and Sebastian Ebert for excellent technical assistance and Dennis May for providing transgenic animals.

For Peer Review

**Figure legends**

**Figure 1. Dye coupling in thalamus.** **A<sub>1</sub>**, Representative current pattern of an EGFP fluorescent astrocyte in hGFAP-EGFP mice. De- and hyperpolarization of the membrane between -160 and +20 mV evoked a passive current pattern in whole-cell voltage clamp mode (10 mV increment, holding potential -80 mV). Scale bar, 10 ms, 5 nA. **A<sub>2</sub>**, Tracer-coupled glial cells, biocytin spread from the initial cell always revealed large networks. **B**, The tracer also diffused along presumed myelinated fiber tracts, as shown in the inset. Scale bar, 50  $\mu$ m. **C**, Summary of the amount of tracer coupling at different time points. The average GJN size increased between p9-11 and p13-15 and was constant during later development. Number of experiments is given in parentheses. Asterisk indicates statistical significance (\* $p < 0.05$ ).

**Figure 2. Astrocyte heterogeneity revealed by network analysis in Cx43kiECFP mice.** **A-C**, ECFP<sup>+</sup> astrocytes in the cortex (CO), CA1 region of the hippocampus (HC) and thalamus (TH) were filled with biocytin. In heterozygous Cx43 (*Gjal*<sup>ECFP/+</sup>) mice, all brains regions investigated displayed tracer-coupled networks (**A<sub>1</sub>**, **B<sub>1</sub>**, **C<sub>1</sub>**), which contained frequent ECFP<sup>+</sup> cells (**A<sub>2</sub>**, **B<sub>2</sub>**, **C<sub>2</sub>**). **A<sub>4</sub>**, **B<sub>4</sub>**, **C<sub>4</sub>**, Blow ups of insets in merged pictures (**A<sub>3</sub>**, **B<sub>3</sub>**, **C<sub>3</sub>**). Colocalization of biocytin and ECFP was observed in many cells in all regions. Scale bars in **C<sub>3</sub>** and **C<sub>4</sub>** indicate 20  $\mu$ m. **D<sub>1</sub>**, Summary of the extent of biocytin coupling in the corresponding brain regions of wild-type littermates (wt) and heterozygous Cx43 (*Gjal*<sup>ECFP/+</sup>) mice (ECFP). **D<sub>2</sub>**, Proportion of tracer-filled cells showing ECFP and biocytin colocalization in the three brain regions (HC, 96.6  $\pm$  0.76 %; CO, 72.6  $\pm$  3.6 %; TH, 43.8  $\pm$  4.6 %). Number of investigated GJNs is shown above bars. **E<sub>1</sub>**, sqRT-PCR amplification curves of Cx43 (*Gjal*, squares) and  $\beta$ -actin mRNA (triangles) obtained from the hippocampus (filled symbols) and thalamus (open symbols). The difference in threshold cycles between  $\beta$ -actin and Cx43 ( $\Delta$ Rn; taken at the dashed line) for the thalamus was larger than for the hippocampus, consistent with lower Cx43 transcript levels in the former. **E<sub>2</sub>**, Transcript ratios



Cx43(*Gja1*)/ $\beta$ -actin and Cx30(*Gjb6*)/ $\beta$ -actin differed significantly between the hippocampus and thalamus. Cx43 expression was higher in the hippocampus while in the thalamus Cx30 predominates. N of tissue specimens in parentheses. Asterisks indicate statistical significance (\* $p < 0.05$ , \*\*  $p < 0.01$ ).

**Figure 3. SR101<sup>+</sup> astrocytes display differential Cx43-ECFP expression in hippocampus**

**and thalamus. A-B,** Two-photon images of SR101 labelled astrocytes in acute brain slices of Cx43<sup>ECFP/+</sup> mice (**A<sub>1-2</sub>**, **B<sub>1-2</sub>**). In both regions colocalization of SR101 and ECFP was observed though to a differing extent (**A<sub>3</sub>**, **B<sub>3</sub>**). Quantifications of the populations of astrocytes are shown in **A<sub>4</sub>** and **B<sub>4</sub>** ( $n = 9$  and  $6$  from  $3$  mice each, respectively). **C-D,** Astrocyte-specific labeling of SR101 was confirmed in PLP-GFP mice. Acute brain slices of PLP-GFP mice were analyzed in similar experiments as Cx43-ECFP mice (**C<sub>1-2</sub>**, **D<sub>1-2</sub>**), showing only minor overlap of PLP-GFP and SR101 in the thalamus (**C<sub>3</sub>**, **C<sub>4</sub>**) or hippocampus (**D<sub>3</sub>**, **D<sub>4</sub>**) ( $n = 11$  and  $8$  from  $4$  and  $3$  mice, respectively). Scale bar,  $20 \mu\text{m}$ .

**Figure 4. Connexin30 is the predominant gap junction protein in the thalamus. A,**

Confocal images of biocytin labelled cells in the thalamus of *Gjb6*<sup>+/+</sup> mice (**A<sub>1</sub>**) and *Gjb6*<sup>LacZ/LacZ</sup> littermates (**A<sub>2</sub>**). *Gjb6*<sup>LacZ/LacZ</sup> littermates displayed smaller or no networks, with a bright initially injected cell and only weakly labelled neighboring cells. **A<sub>3</sub>**, Networks sizes were decreased by  $73\%$  in *Gjb6*<sup>LacZ/LacZ</sup> vs. *Gjb6*<sup>+/+</sup> mice. Number of experiments is given in parentheses. **B,** Mice heterozygous for Cx30kiLacZ (**B<sub>1</sub>**) and for Cx43kiECFP (**B<sub>2</sub>**) were immunohistochemically analyzed for reporter gene expression in the thalamus. Different populations were observed according to their connexin expression profile. Most cells showed colocalization of the reporters (yellow), but cells expressing only one reporter were also present (red or green) (**B<sub>3</sub>**, merge). **B<sub>4</sub>**, Quantitative summary of connexin reporter expression revealed three different astrocytic populations in the thalamus, almost all cells investigated

expressed Cx30 ( $\beta\text{Gal}^+/\text{ECFP}^+$ ,  $78.1 \pm 2.6\%$ ;  $\beta\text{Gal}^+/\text{ECFP}^-$ ,  $20.4 \pm 2.4\%$ ;  $\beta\text{Gal}^-/\text{ECFP}^+$ ,  $1.5 \pm 0.7\%$ ,  $n = 9$  from 3 mice). Scale bar,  $20\ \mu\text{m}$ . **C<sub>1</sub>**, Western blot analysis of Cx30 protein levels in the thalamus and hippocampus of C57/Bl6 mice at two different time points. Cx30 protein levels increased with age and differ between the two brain regions. Antibody specificity was confirmed using the Cx30/Cx43 (*Gjb6*<sup>LacZ/LacZ</sup>; *Gja1*<sup>fl/fl</sup>; *hGFAP-Cre*) double-knockout mouse (DKO) as negative control,  $\beta$ -tubulin as a loading control. **C<sub>2</sub>**, Normalized protein levels confirmed the increase of Cx30 levels during development, although this was more pronounced in the thalamus. **D<sub>1</sub>**, Western blot analysis of Cx43 (C57/Bl6), the two bands visible correspond to different phosphorylation status of the protein. **D<sub>2</sub>**, Cx43 protein levels were normalized to  $\beta$ -tubulin levels, yielding a lower expression in the thalamus at p14, while in adult animals no difference in Cx43 expression was detected. (**C<sub>2</sub>**, **D<sub>2</sub>**; number of mice above bars). Asterisks indicate statistical significance.

**Figure 5. Tracer-coupled GJN have distinct immunohistochemical properties.**

Immunostainings of GJNs (**A<sub>1</sub>-E<sub>1</sub>**) in hGFAP-EGFP mice in the thalamus, hippocampus and cortex using antibodies against GS (**A<sub>2</sub>**, **B<sub>2</sub>**) and Olig2 (**C<sub>2</sub>**, **D<sub>2</sub>**, **E<sub>2</sub>**). **A<sub>3</sub>-E<sub>3</sub>** show merged images. Note that networks in the thalamus contained less than 50% GS<sup>+</sup> cells (**A<sub>4</sub>**,  $46.4 \pm 5.4\%$ ,  $n = 10$ ) but most coupled cells in this region were Olig2<sup>+</sup> (**C<sub>4</sub>**,  $62.2 \pm 8.4\%$ ,  $n = 10$ ). In contrast, hippocampal GJNs mainly comprised GS<sup>+</sup> cells (**B<sub>4</sub>**,  $81.6 \pm 2\%$ ,  $n = 7$ ), while only a few cells were Olig2<sup>+</sup> (**D<sub>4</sub>**,  $17.5 \pm 4.6\%$ ,  $n = 7$ ). Similar to the thalamus, most of the coupled cells in the neocortex were Olig2<sup>+</sup> (**E<sub>4</sub>**,  $60 \pm 15\%$ ,  $n = 8$ ). Scale bar,  $20\ \mu\text{m}$ .

**Figure 6: Astrocyte:Oligodendrocyte coupling is independent of the initial filled cell-**

**type. A-D**, Astrocytes and oligodendrocytes in the thalamus and hippocampus of PLP-GFP mice were identified by SR101 labelling or GFP fluorescence, accordingly. Either astrocytes (**A**, **C**; indicated by AC) or oligodendrocytes (**B**, **D**; as indicated by OL) were tracer-filled

(A<sub>1</sub>-D<sub>1</sub>) and co-stained for GFP (A<sub>2</sub>-D<sub>2</sub>) revealing spread of the tracer into PLP-GFP<sup>+</sup> oligodendrocytes (A<sub>3</sub>-C<sub>3</sub>). Notably, all PLP-GFP<sup>+</sup> oligodendrocytes injected in the thalamus or hippocampus showed intercellular coupling (B<sub>3</sub>, D<sub>3</sub>). Scale bar, 20  $\mu$ m. E<sub>1</sub>, Graph showing the number of coupled cells in the thalamus and hippocampus, depending on whether the injected cell was an astrocyte (AC) or an oligodendrocyte (OL). Size of the GJNs did not differ significantly. E<sub>2</sub>, The proportion of PLP-GFP<sup>+</sup> cells in the networks was larger in the thalamus, but independent of the cell type initially filled with the tracer (TH,  $53.1 \pm 6.4\%$  and  $66.5 \pm 8.4\%$ , HC:  $12.4 \pm 1$  and  $13.4 \pm 1.4$ , injection into AC or OL, respectively). Number of experiments is given above bars. Asterisks indicate statistical significance.

**Figure 7: Panglial networks require Cx30 and Cx47 in the thalamus.** Astrocytes in Cx30kiLacZ;Cx47kiEGFP mice were identified for tracer injection with SR101. Analysis of biocytin-filled networks (red) for the presence of Cx47-EGFP (green) and Cx30-LacZ (blue) expressing cells in *Gjb6*<sup>+/LacZ</sup>; *Gjc2*<sup>EGFP/EGFP</sup> mice revealed panglial networks (A<sub>1</sub>) while coupling was lacking or drastically reduced in homozygous Cx30/Cx47 (*Gjb6*<sup>LacZ/LacZ</sup>; *Gjc2*<sup>EGFP/EGFP</sup>) mice (A<sub>2</sub>). Examples depict networks in the thalamus. Scale bar, 20  $\mu$ m. (B) Three genotypes were analyzed both in hippocampus and thalamus for the proportion of coupled and uncoupled cells. (C) Analysis of network size revealed minimal tracer spread in Cx30/Cx47 deficient mice. (D) Proportion of Cx47-EGFP<sup>+</sup> oligodendrocytes. Note that oligodendrocytes were lacking in GJNs of Cx30/Cx47 deficient mice. Asterisks indicate statistical significance, number of experiments is given in parentheses.

**Figure 8. Thalamic Cx43-ECFP<sup>+</sup> cells express the oligodendrocyte marker Olig2.** Immunostaining for Olig2 in thalamus (A<sub>1</sub>) and hippocampus (B<sub>1</sub>) was performed in heterozygous Cx43 (*Gjal*<sup>ECFP/+</sup>) mice (A<sub>2</sub>, B<sub>2</sub>). Merged images (A<sub>3</sub>, B<sub>3</sub>) show a large overlap of ECFP and Olig2 staining in the thalamus, while in the hippocampus only very few

ECFP<sup>+</sup>/Olig2<sup>+</sup> cells were observed. Scale bar, 20 μm. **A<sub>4</sub>**, **B<sub>4</sub>**, Quantitative analysis of the ECFP and Olig2 expression profile confirmed a significant differences in the antigen profile of astrocytes in both regions (overlap TH, 52.2 ± 6 %; HC, 6 ± 1.8 %, n = 9 for each region from 3 mice).

**Author Contributions**

SG, SH, GS, MT, HK and CS designed the research. SG, SH, GS, and CS wrote the manuscript. SG, SH, PB, JZ, EvS, RJ, NR conducted experiments and analyzed data. JD, PD, VC, DC and KW provided new methods/reagents or tools.

**Reference List**

Bokor H, Acsady L, Deschenes M. 2008. Vibrissal responses of thalamic cells that project to the septal columns of the barrel cortex and to the second somatosensory area. *J Neurosci* 28:5169-5177.

Bourassa J, Pinault D, Deschenes M. 1995. Corticothalamic projections from the cortical barrel field to the somatosensory thalamus in rats: a single-fibre study using biocytin as an anterograde tracer. *Eur J Neurosci* 7:19-30.

Cai J, Chen Y, Cai WH, Hurlock EC, Wu H, Kernie SG, Parada LF, Lu QR. 2007. A crucial role for Olig2 in white matter astrocyte development. *Development* 134:1887-1899.

Cammer W. 1990. Glutamine synthetase in the central nervous system is not confined to astrocytes. *J Neuroimmunol* 26:173-178.

Coulter DA, Eid T. 2012. Astrocytic regulation of glutamate homeostasis in epilepsy. *Glia* 60:1215-1226.

Crunelli V, Hughes SW. 2010. The slow (<1 Hz) rhythm of non-REM sleep: a dialogue between three cardinal oscillators. *Nat Neurosci* 13:9-17.

D'Amelio F, Eng LF, Gibbs MA. 1990. Glutamine synthetase immunoreactivity is present in oligodendroglia of various regions of the central nervous system. *Glia* 3:335-341.

Degen J, Dublin P, Zhang J, Dobrowolski R, Jokwitz M, Karram K, Trotter J, Jabs R, Willecke K, Steinhäuser C, Theis M. 2012. Dual reporter approaches for identification of Cre efficacy and astrocyte heterogeneity. *FASEB J* 26:4576-4583.

- Dermietzel R, Traub O, Hwang TK, Beyer E, Bennett MVL, Spray DC, Willecke K. 1989. Differential expression of the three gap junction proteins in developing and mature brain tissues. *Proc Natl Acad Sci USA* 86:10148-10152.
- Derouiche A, Frotscher M. 1991. Astroglial processes around identified glutamatergic synapses contain glutamine synthetase: evidence for transmitter degradation. *Brain Res* 552:346-350.
- Elfgang C, Eckert R, Lichtenberg-Frate H, Butterweck A, Traub O, Klein RA, Hulser DF, Willecke K. 1995. Specific permeability and selective formation of gap junction channels in connexin-transfected HeLa cells. *J Cell Biol* 129:805-817.
- Frasconi C, Amadeo A, Ortino B, Jaranowska A, Spreafico R. 2000. Organization of radial and non-radial glia in the developing rat thalamus. *J Comp Neurol* 428:527-542.
- Funfschilling U, Supplie LM, Mahad D, Boretius S, Saab AS, Edgar J, Brinkmann BG, Kassmann CM, Tzvetanova ID, Mobius W, Diaz F, Meijer D, Suter U, Hamprecht B, Sereda MW, Moraes CT, Frahm J, Goebbels S, Nave KA. 2012. Glycolytic oligodendrocytes maintain myelin and long-term axonal integrity. *Nature* 485:517-521.
- Fuss B, Mallon B, Phan T, Ohlemeyer C, Kirchhoff F, Nishiyama A, Macklin WB. 2000. Purification and analysis of *in vivo*-differentiated oligodendrocytes expressing the green fluorescent protein. *Dev Biol* 218:259-274.
- Giaume C, Koulakoff A, Roux L, Holcman D, Rouach N. 2010. Astroglial networks: a step further in neuroglial and gliovascular interactions. *Nat Rev Neurosci* 11:87-99.
- Gosejacob D, Dublin P, Bedner P, Hüttmann K, Zhang J, Tress O, Willecke K, Pfrieger F, Steinhäuser C, Theis M. 2011. Role of astroglial connexin30 in hippocampal gap junction coupling. *Glia* 59:511-519.
- Houades V, Koulakoff A, Ezan P, Seif I, Giaume C. 2008. Gap junction-mediated astrocytic networks in the mouse barrel cortex. *J Neurosci* 28:5207-5217.
- Kafitz KW, Meier SD, Stephan J, Rose CR. 2008. Developmental profile and properties of sulforhodamine 101-labelled glial cells in acute brain slices of rat hippocampus. *J Neurosci Methods* 169:84-92.
- Kunzelmann P, Schröder W, Traub O, Steinhäuser C, Dermietzel R, Willecke K. 1999. Late onset and increasing expression of the gap junction protein connexin30 in adult murine brain and long-term cultured astrocytes. *Glia* 25:111-119.
- Lee Y, Morrison BM, Li Y, Lengacher S, Farah MH, Hoffman PN, Liu Y, Tsingalia A, Jin L, Zhang PW, Pellerin L, Magistretti PJ, Rothstein JD. 2012. Oligodendroglia metabolically support axons and contribute to neurodegeneration. *Nature* 487:443-448.
- Li X, Penes M, Odermatt B, Willecke K, Nagy JI. 2008. Ablation of Cx47 in transgenic mice leads to the loss of MUPP1, ZONAB and multiple connexins at oligodendrocyte-astrocyte gap junctions. *Eur J Neurosci* 28:1503-1517.
- Maglione M, Tress O, Haas B, Karam K, Trotter J, Willecke K, Kettenmann H. 2010. Oligodendrocytes in mouse corpus callosum are coupled via gap junction channels formed by connexin47 and connexin32. *Glia* 58:1104-1117.

Magnotti LM, Goodenough DA, Paul DL. 2011. Functional heterotypic interactions between astrocyte and oligodendrocyte connexins. *Glia* 59:26-34.

Marshall CA, Novitch BG, Goldman JE. 2005. Olig2 directs astrocyte and oligodendrocyte formation in postnatal subventricular zone cells. *J Neurosci* 25:7289-7298.

Matthias K, Kirchhoff F, Seifert G, Hüttmann K, Matyash M, Kettenmann H, Steinhäuser C. 2003. Segregated expression of AMPA-type glutamate receptors and glutamate transporters defines distinct astrocyte populations in the mouse hippocampus. *J Neurosci* 23:1750-1758.

Matyash V, Kettenmann H. 2010. Heterogeneity in astrocyte morphology and physiology. *Brain Res Rev* 63:2-10.

May D, Tress O, Seifert G, Willecke K. 2013. Connexin47 protein phosphorylation and stability in oligodendrocytes depend on expression of Connexin43 protein in astrocytes. *J Neurosci* 33:7985-7996.

Menichella DM, Goodenough DA, Sirkowski E, Scherer SS, Paul DL. 2003. Connexins are critical for normal myelination in the CNS. *J Neurosci* 23:5963-5973.

Miyake T, Kitamura T. 1992. Glutamine synthetase immunoreactivity in two types of mouse brain glial cells. *Brain Res* 586:53-60.

Nagy JJ, Li X, Rempel J, Stelmack G, Patel D, Staines WA, Yasumura T, Rash JE. 2001. Connexin26 in adult rodent central nervous system: demonstration at astrocytic gap junctions and colocalization with connexin30 and connexin43. *J Comp Neurol* 441:302-323.

Nagy JJ, Lynn BD, Tress O, Willecke K, Rash JE. 2011. Connexin26 expression in brain parenchymal cells demonstrated by targeted connexin ablation in transgenic mice. *Eur J Neurosci* 34:263-271.

Nagy JJ, Ochalski PAY, Li J, Hertzberg EL. 1997. Evidence for the co-localization of another connexin with connexin-43 at astrocytic gap junctions in rat brain. *Neuroscience* 78:533-548.

Nagy JJ, Rash JE. 2000. Connexins and gap junctions of astrocytes and oligodendrocytes in the CNS. *Brain Res Rev* 32:29-44.

Nave KA. 2010. Myelination and support of axonal integrity by glia. *Nature* 468:244-252.

Nimmerjahn A, Kirchhoff F, Kerr JN, Helmchen F. 2004. Sulforhodamine 101 as a specific marker of astroglia in the neocortex in vivo. *Nat Methods* 1:31-37.

Nishiyama A, Komitova M, Suzuki R, Zhu X. 2009. Polydendrocytes (NG2 cells): multifunctional cells with lineage plasticity. *Nat Rev Neurosci* 10:9-22.

Nolte C, Matyash M, Pivneva T, Schipke CG, Ohlemeyer C, Hanisch UK, Kirchhoff F, Kettenmann H. 2001. GFAP promoter-controlled EGFP-expressing transgenic mice: A tool to visualize astrocytes and astrogliosis in living brain tissue. *Glia* 33:72-86.

Norenberg MD. 1979. Distribution of glutamine synthetase in the rat central nervous system. *J Histochem Cytochem* 27:756-762.



- Nualart-Martí A, Solsona C, Fields RD. 2013. Gap junction communication in myelinating glia. *Biochim Biophys Acta* 1828:69-78.
- Odermatt B, Wellershaus K, Wallraff A, Seifert G, Degen J, Euwens C, Fuss B, Bussow H, Schilling K, Steinhäuser C, Willecke K. 2003. Connexin 47 (cx47)-deficient mice with enhanced green fluorescent protein reporter gene reveal predominant oligodendrocytic expression of cx47 and display vacuolized myelin in the CNS. *J Neurosci* 23:4549-4559.
- Ogata K, Kosaka T. 2002. Structural and quantitative analysis of astrocytes in the mouse hippocampus. *Neuroscience* 113:221-233.
- Ono K, Takebayashi H, Ikeda K, Furusho M, Nishizawa T, Watanabe K, Ikenaka K. 2008. Regional- and temporal-dependent changes in the differentiation of Olig2 progenitors in the forebrain, and the impact on astrocyte development in the dorsal pallium. *Dev Biol* 320:456-468.
- Orthmann-Murphy JL, Freidin M, Fischer E, Scherer SS, Abrams CK. 2007. Two Distinct Heterotypic Channels Mediate Gap Junction Coupling between Astrocyte and Oligodendrocyte Connexins. *J Neurosci* 27:13949-13957.
- Pannasch U, Rouach N. 2013. Emerging role for astroglial networks in information processing: from synapse to behavior. *Trends Neurosci* 36:405-417.
- Pannasch U, Vargova L, Reingruber J, Ezan P, Holcman D, Giaume C, Sykova E, Rouach N. 2011. Astroglial networks scale synaptic activity and plasticity. *Proc Natl Acad Sci U S A* 108:8467-8472.
- Parri HR, Crunelli V. 2002. Astrocytes, spontaneity, and the developing thalamus. *J Physiol Paris* 96:221-230.
- Parri HR, Gould TM, Crunelli V. 2001. Spontaneous astrocytic Ca<sup>2+</sup> oscillations in situ drive NMDAR-mediated neuronal excitation. *Nat Neurosci* 4:803-812.
- Parri HR, Gould TM, Crunelli V. 2010. Sensory and cortical activation of distinct glial cell subtypes in the somatosensory thalamus of young rats. *Eur J Neurosci* 32:29-40.
- Pellerin L, Magistretti PJ. 2012. Sweet sixteen for ANLS. *J Cereb Blood Flow Metab* 32:1152-1166.
- Pirttimäki TM, Hall SD, Parri HR. 2011. Sustained neuronal activity generated by glial plasticity. *J Neurosci* 31:7637-7647.
- Pirttimäki TM, Parri HR, Crunelli V. 2013. Astrocytic GAT-1 dysfunction in experimental absence seizures. *J Physiol* 591:823-833..
- Requardt RP, Kaczmarczyk L, Dublin P, Wallraff-Beck A, Mikeska T, Degen J, Waha A, Steinhäuser C, Willecke K, Theis M. 2009. Quality control of astrocyte-directed Cre transgenic mice: The benefits of a direct link between loss of gene expression and reporter activation. *Glia* 57:680-692.
- Rouach N, Koulakoff A, Abudara V, Willecke K, Giaume C. 2008. Astroglial metabolic networks sustain hippocampal synaptic transmission. *Science* 322:1551-1555.



Roux L, Benchenane K, Rothstein JD, Bonvento G, Giaume C. 2011. Plasticity of astroglial networks in olfactory glomeruli. *Proc Natl Acad Sci U S A* 108:18442-18446.

Schools GP, Zhou M, Kimelberg HK. 2006. Development of gap junctions in hippocampal astrocytes: evidence that whole cell electrophysiological phenotype is an intrinsic property of the individual cell. *J Neurophysiol* 96:1383-1392.

Sonnwald U, Westergaard N, Schousboe A. 1997. Glutamate transport and metabolism in astrocytes. *Glia* 21:56-63.

Steriade M. 2006. Grouping of brain rhythms in corticothalamic systems. *Neuroscience* 137:1087-1106.

Suzuki A, Stern SA, Bozdagi O, Huntley GW, Walker RH, Magistretti PJ, Alberini CM. 2011. Astrocyte-neuron lactate transport is required for long-term memory formation. *Cell* 144:810-823.

Takasaki C, Yamasaki M, Uchigashima M, Konno K, Yanagawa Y, Watanabe M. 2010. Cytochemical and cytological properties of perineuronal oligodendrocytes in the mouse cortex. *Eur J Neurosci* 32:1326-1336.

Teubner B, Michel V, Pesch J, Lautermann J, Cohen-Salmon M, Sohl G, Jahnke K, Winterhager E, Herberhold C, Hardelin JP, Petit C, Willecke K. 2003. Connexin30 (Gjb6)-deficiency causes severe hearing impairment and lack of endocochlear potential. *Hum Mol Genet* 12:13-21.

Theis M, Giaume C. 2012. Connexin-based intercellular communication and astrocyte heterogeneity. *Brain Res* 1487:88-98.

Tress O, Maglione M, May D, Pivneva T, Richter N, Seyfarth J, Binder S, Zlomuzica A, Seifert G, Theis M, Dere E, Kettenmann H, Willecke K. 2012. Panglial gap junctional communication is essential for maintenance of myelin in the CNS. *J Neurosci* 32:7499-7518.

Tress O, Maglione M, Zlomuzica A, May D, Dicke N, Degen J, Dere E, Kettenmann H, Hartmann D, Willecke K. 2011. Pathologic and phenotypic alterations in a mouse expressing a connexin47 missense mutation that causes Pelizaeus-Merzbacher-like disease in humans. *PLoS Genet* 7:e1002146.

Trotter J, Karram K, Nishiyama A. 2010. NG2 cells: Properties, progeny and origin. *Brain Res Rev* 63:72-82.

Uhlenberg B, Schuelke M, Ruschendorf F, Ruf N, Kaendl AM, Henneke M, Thiele H, Stoltenburg-Diding G, Aksu F, Topaloglu H, Nurnberg P, Hubner C, Weschke B, Gartner J. 2004. Mutations in the gene encoding gap junction protein alpha 12 (connexin 46.6) cause Pelizaeus-Merzbacher-like disease. *Am J Hum Genet* 75:251-260.

Wallraff A, Kohling R, Heinemann U, Theis M, Willecke K, Steinhäuser C. 2006. The impact of astrocytic gap junctional coupling on potassium buffering in the hippocampus. *J Neurosci* 26:5438-5447.

Wasseff SK, Scherer SS. 2011. Cx32 and Cx47 mediate oligodendrocyte:astrocyte and oligodendrocyte:oligodendrocyte gap junction coupling. *Neurobiol Dis* 42:506-513.

Yum SW, Zhang J, Valiunas V, Kanaporis G, Brink PR, White TW, Scherer SS. 2007.  
Human connexin26 and connexin30 form functional heteromeric and heterotypic channels.  
Am J Physiol Cell Physiol 293:C1032-C1048.

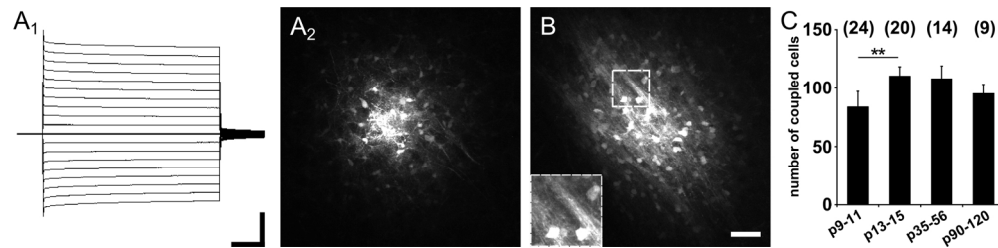
Zhang Y, Barres BA. 2010. Astrocyte heterogeneity: an underappreciated topic in  
neurobiology. Curr Opin Neurobiol 20:588-594.

For Peer Review

Table 1: Primers for semi-quantitative RT-PCR

Gene	Sequence	Position	Product length	GeneBank Accession No.
<i>Gjal</i> (Cx43)	se 5'-TTTGACTTCAGCCTCCAAGGA	-80	79 bp	NM_010288
	as 5'-TCTGGGCACCTCTCTTTCACTTA	-24		
<i>Gjal</i> (Cx43) probe	se 5'-TTCCACCACTTTGGCGTGCCG	-58		
<i>Gjb6</i> (Cx30)	se CGTACACCAGCAGCATTTTCTT	404	78 bp	NM_001010937
	as 5'-ACCCATTGTAGAGGAAGTAGAACACAT	455		
<i>Gjb6</i> (Cx30) probe	se 5'-CGCATCATCTTCGAAGCCGCCT	427		

‘Se’ and ‘as’ mark sense and antisense primers. Position 1 is the first nucleotide of the initiation codon. The fluorogenic TaqMan *Gjb6* (Cx30 )and *Gjal*(Cx43) probes were labeled at their 5’-end with 6-carboxyfluoresceine (FAM) and at their 3’-end with 6-carboxytetramethylrhodamine (TAMRA).



Dye coupling in thalamus. A1, Representative current pattern of an EGFP fluorescent astrocyte in hGFAP-EGFP mice. De- and hyperpolarization of the membrane between -160 and +20 mV evoked a passive current pattern in whole-cell voltage clamp mode (10 mV increment, holding potential -80 mV). Scale bar, 10 ms, 5 nA. A2, Tracer-coupled glial cells, biocytin spread from the initial cell always revealed large networks. B, The tracer also diffused along presumed myelinated fiber tracts, as shown in the inset. Scale bar, 50  $\mu$ m. C, Summary of the amount of tracer coupling at different time points. The average GJN size increased between p9-11 and p13-15 and was constant during later development. Number of experiments is given in parentheses. Asterisk indicates statistical significance (\* $p < 0.05$ ).

180x43mm (299 x 299 DPI)

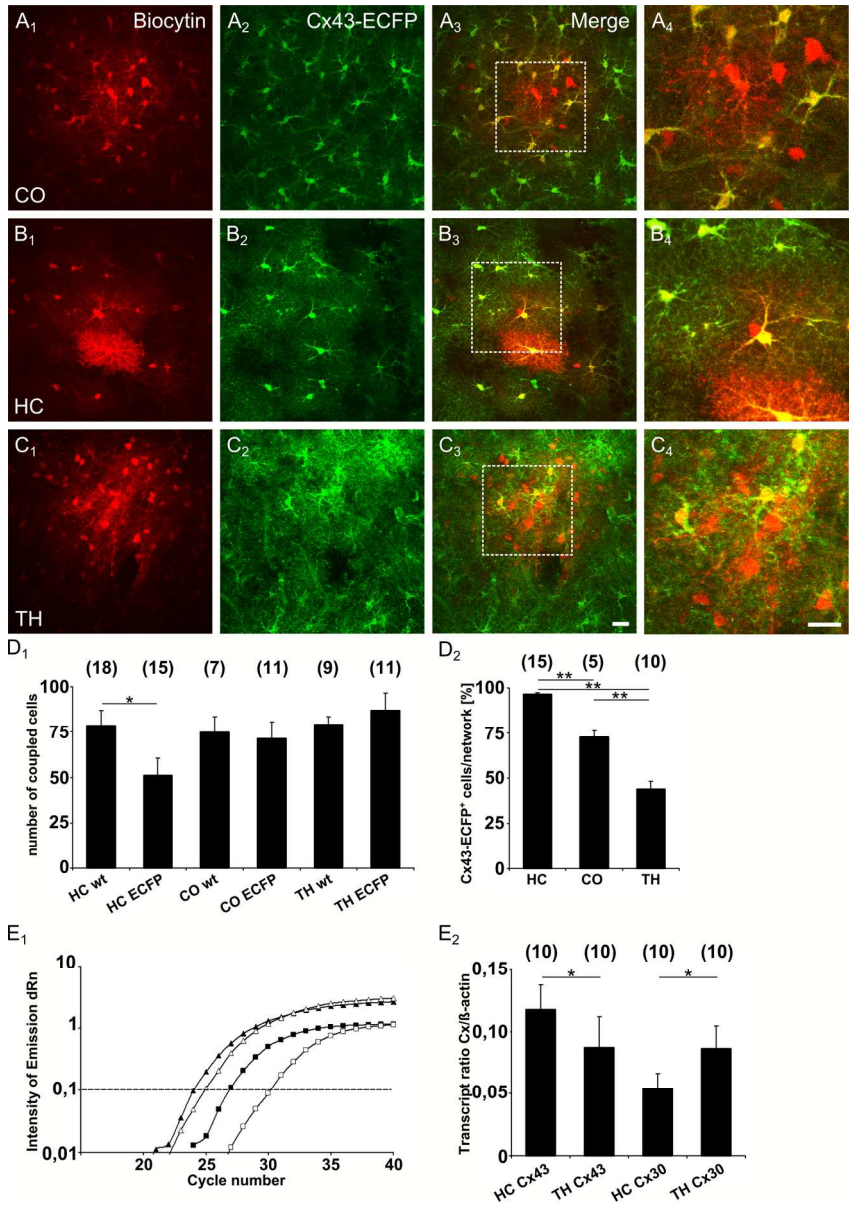


Figure 2. Astrocyte heterogeneity revealed by network analysis in Cx43kiECFP mice. A-C, ECFP+ astrocytes in the cortex (CO), CA1 region of the hippocampus (HC) and thalamus (TH) were filled with biocytin. In Cx43ECFP/+ mice, all brains regions investigated displayed tracer-coupled networks (A1, B1, C1), which contained frequent ECFP+ cells (A2,, B2 , C2). A4, B4, C4, Blow ups of insets in merged pictures (A3, B3, C3). Colocalization of biocytin and ECFP was observed in many cells in all regions. Scale bars in C3 and C4 indicate 20  $\mu$ m. D1, Summary of the extent of biocytin coupling in the corresponding brain regions of wild-type littermates (wt) and heterozygous Cx43ECFP/+ mice (ECFP). D2, Proportion of tracer-filled cells showing ECFP and biocytin colocalization in the three brain regions (HC, 96.6  $\pm$  0.76 %; CO, 72.6  $\pm$  3.6 %; TH, 43.8  $\pm$  4.6 %). Number of investigated GJNs is shown above bars. E1, sqRT-PCR amplification curves of Cx43 (squares) and  $\beta$ -actin mRNA (triangles) obtained from the hippocampus (filled symbols) and thalamus (open symbols). The difference in threshold cycles between  $\beta$ -actin and Cx43 ( $\Delta$ Rn; taken at the dashed line) for the thalamus was larger than for the hippocampus, consistent with lower Cx43 transcript levels in the former. E2, Transcript ratios Cx43/ $\beta$ -actin and Cx30/ $\beta$ -actin differed significantly between the

hippocampus and thalamus. Cx43 expression was higher in the hippocampus while in the thalamus Cx30 predominates. N of tissue specimens in parentheses. Asterisks indicate statistical significance (\* $p < 0.05$ , \*\* $p < 0.01$ ).

150x214mm (299 x 299 DPI)

For Peer Review

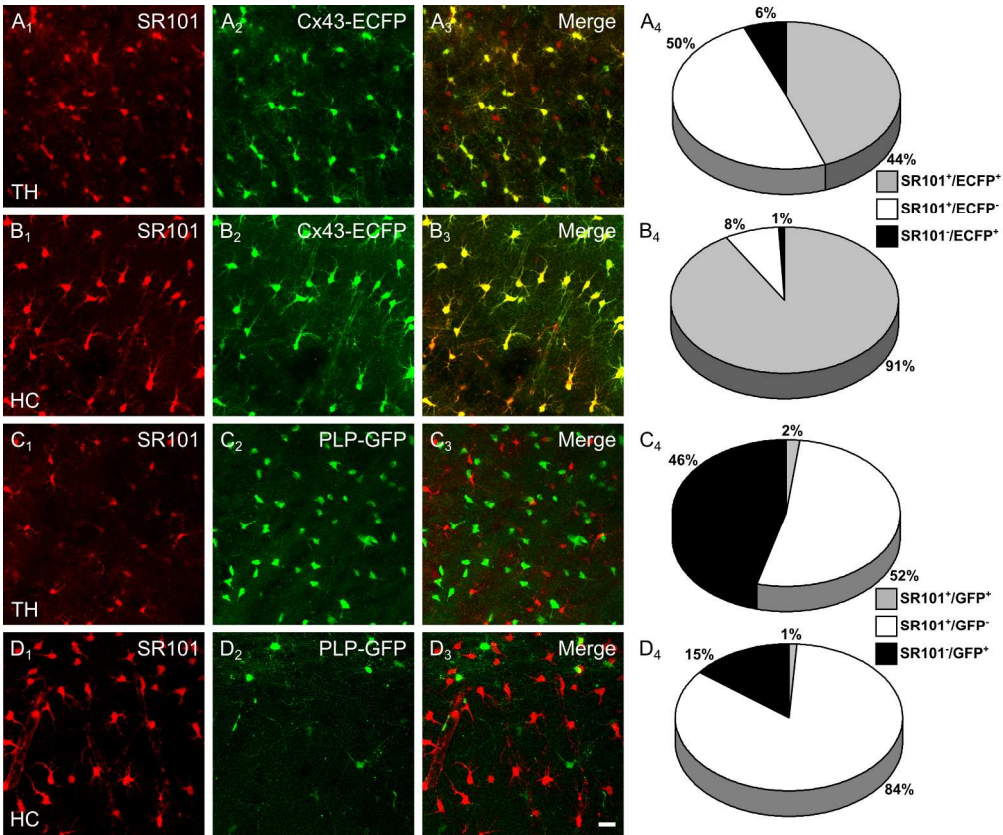


Figure 3. SR101+ astrocytes display differential Cx43-ECFP expression in hippocampus and thalamus. A-B, Two-photon images of SR101 labelled astrocytes in acute brain slices of Cx43ECFP/+ mice (A1-2, B1-2,). In both regions colocalization of SR101 and ECFP was observed though to a differing extent (A3, B3). Quantifications of the populations of astrocytes are shown in A4 and B4 (n = 9 and 6 from 3 mice each, respectively). C-D, Astrocyte-specific labeling of SR101 was confirmed in PLP-GFP mice. Acute brain slices of PLP-GFP mice were analyzed in similar experiments as Cx43-ECFP mice (C1-2, D1-2), showing only minor overlap of PLP-GFP and SR101 in the thalamus (C3, C4) or hippocampus (D3, D4) (n = 11 and 8 from 4 and 3 mice, respectively). Scale bar, 20 μm. 218x181mm (299 x 299 DPI)



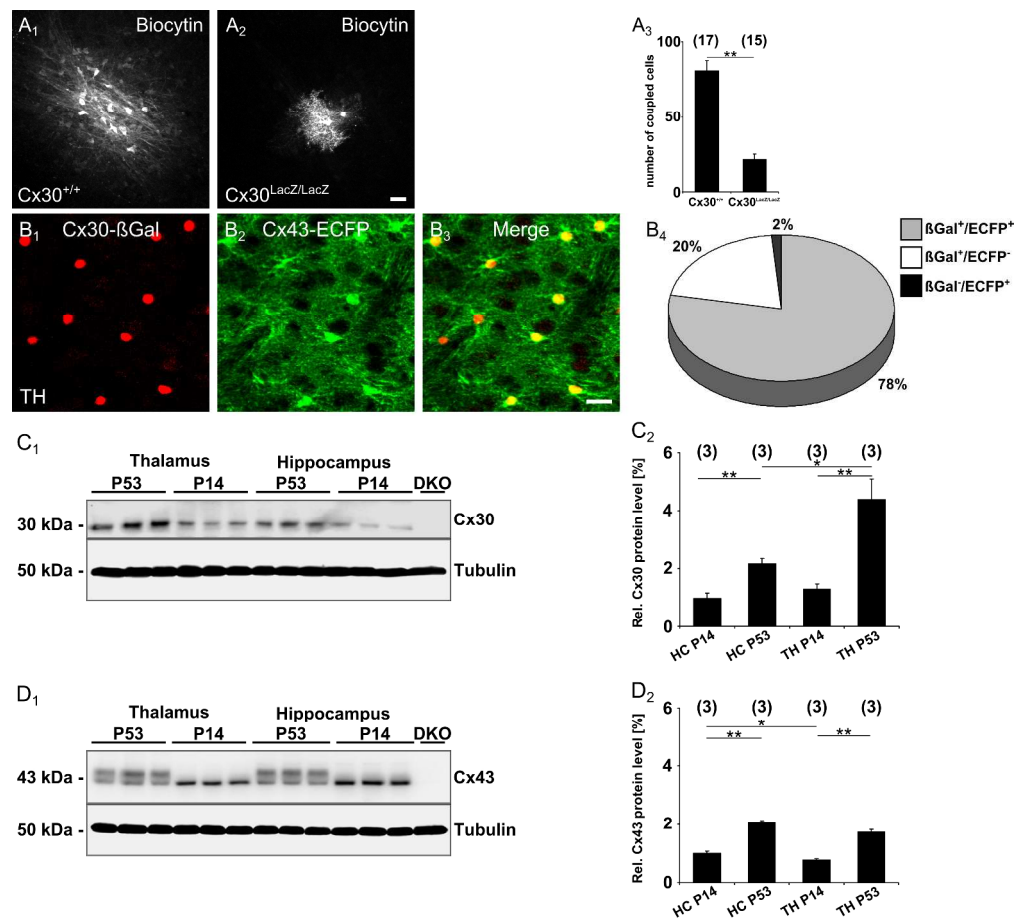


Figure 4. Connexin30 is the predominant gap junction protein in the thalamus. A, Confocal images of biocytin labelled cells in the thalamus of Cx30<sup>+/+</sup> mice (A<sub>1</sub>) and Cx30<sup>LacZ/LacZ</sup> littermates (A<sub>2</sub>). Cx30<sup>LacZ/LacZ</sup> littermates displayed smaller or no networks, with a bright initially injected cell and only weakly labelled neighboring cells. A<sub>3</sub>, Networks sizes were decreased by 73% in Cx30<sup>LacZ/LacZ</sup> vs. Cx30<sup>+/+</sup> mice. Number of experiments is given in parentheses. B, Mice heterozygous for Cx30<sup>kiLacZ</sup> (B<sub>1</sub>) and for Cx43<sup>kiECFP</sup> (B<sub>2</sub>) were immunohistochemically analyzed for reporter gene expression in the thalamus. Different populations were observed according to their connexin expression profile. Most cells showed colocalization of the reporters (yellow), but cells expressing only one reporter were also present (red or green) (B<sub>3</sub>, merge). B<sub>4</sub>, Quantitative summary of connexin reporter expression revealed three different astrocytic populations in the thalamus, almost all cells investigated expressed Cx30 (βGal<sup>+</sup>/ECFP<sup>+</sup>, 78.1 ± 2.6 %; βGal<sup>+</sup>/ECFP<sup>-</sup>, 20.4 ± 2.4 %; βGal<sup>-</sup>/ECFP<sup>+</sup>, 1.5 ± 0.7 %, n = 9 from 3 mice). Scale bar, 20 μm. C<sub>1</sub>, Western blot analysis of Cx30 protein levels in the thalamus and hippocampus of C57/Bl6 mice at two different time points. Cx30 protein levels increased with age and differ between the two brain regions. Antibody specificity was confirmed using the Cx30<sup>LacZ/LacZ</sup>;Cx43<sup>fl/fl</sup>;hGFAP-Cre double-knockout mouse (DKO) as negative control, β-tubulin as a loading control. C<sub>2</sub>, Normalized protein levels confirmed the increase of Cx30 levels during development, although this was more pronounced in the thalamus. D<sub>1</sub>, Western blot analysis of Cx43 (C57/Bl6), the two bands visible correspond to different phosphorylation status of the protein. D<sub>2</sub>, Cx43 protein levels were normalized to β-tubulin levels, yielding a lower expression in the thalamus at p14, while in adult animals no difference in Cx43 expression was detected. (C<sub>2</sub>, D<sub>2</sub>; number of mice above bars). Asterisks indicate statistical significance.

397x362mm (299 x 299 DPI)

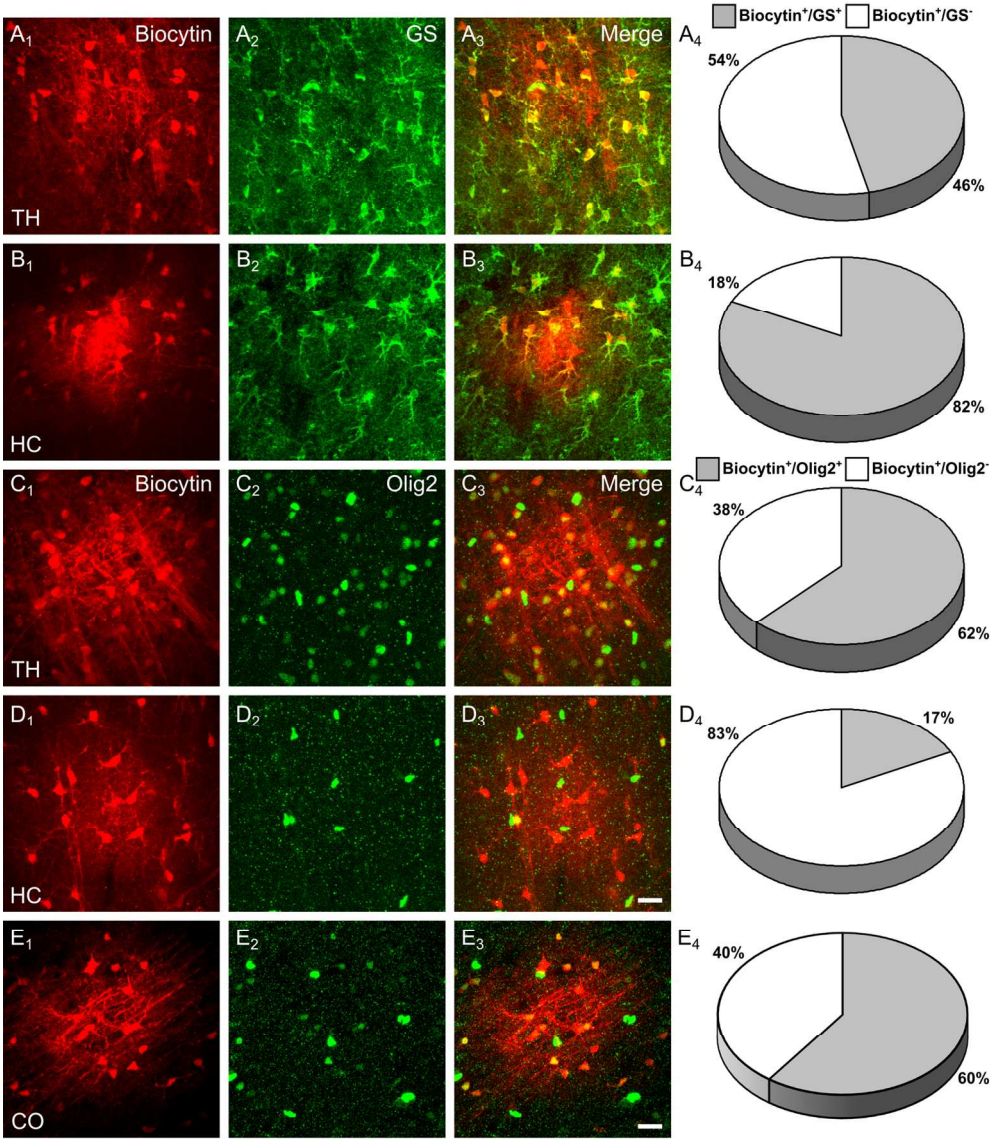


Figure 5. Tracer-coupled GJN have distinct immunohistochemical properties. Immunostainings of GJNs (A1-E1) in hGFAP-EGFP mice in the thalamus, hippocampus and cortex using antibodies against GS (A2, B2) and Olig2 (C2, D2, E2). A3-E3 show merged images. Note that networks in the thalamus contained less than 50% GS+ cells (A4,  $46.4 \pm 5.4$  %,  $n = 10$ ) but most coupled cells in this region were Olig2+ (C4,  $62.2 \pm 8.4$  %,  $n = 10$ ). In contrast, hippocampal GJNs mainly comprised GS+ cells (B4,  $81.6 \pm 2$  %,  $n = 7$ ), while only a few cells were Olig2+ (D4,  $17.5 \pm 4.6$  %,  $n = 7$ ). Similar to the thalamus, most of the coupled cells in the neocortex were Olig2+ (E4,  $60 \pm 15$  %,  $n = 8$ ). Scale bar, 20  $\mu$ m.

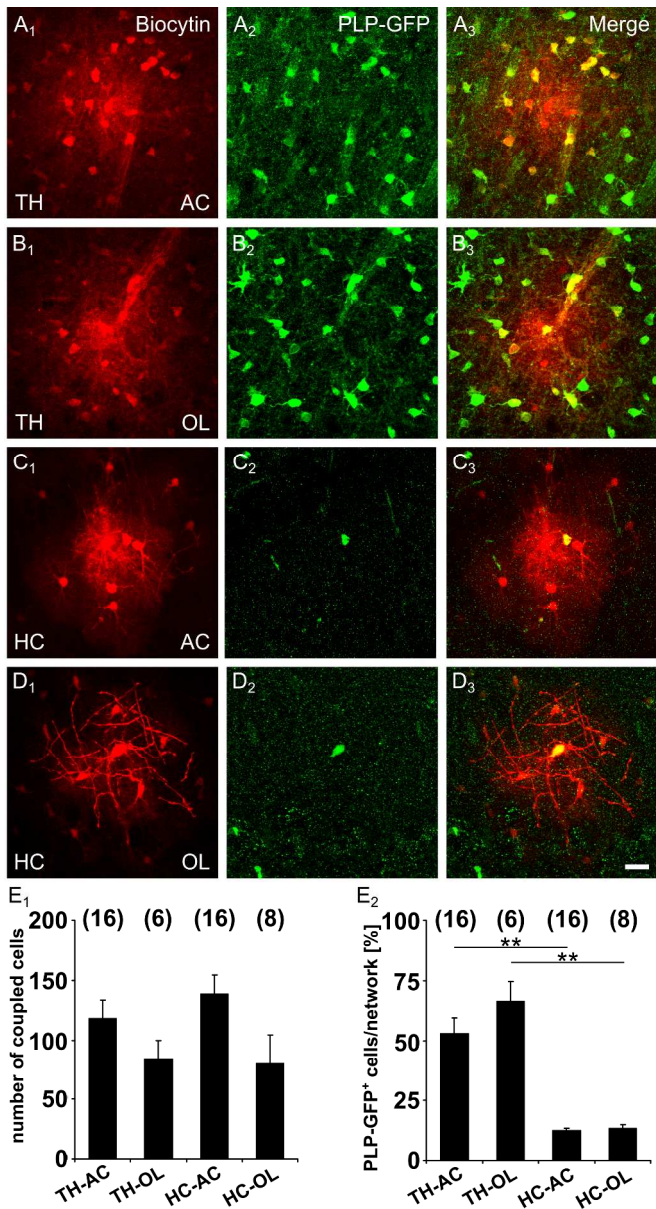


Figure 6. Astrocyte:Oligodendrocyte coupling is independent of the initial filled cell-type. A-D, Astrocytes and oligodendrocytes in the thalamus and hippocampus of PLP-GFP mice were identified by SR101 labelling or GFP fluorescence, accordingly. Either astrocytes (A, C; indicated by AC) or oligodendrocytes (B, D; as indicated by OL) were tracer-filled (A1-D1) and co-stained for GFP (A2-D2) revealing spread of the tracer into PLP-GFP+ oligodendrocytes (A3-C3). Notably, all PLP-GFP+ oligodendrocytes injected in the thalamus or hippocampus showed intercellular coupling (B3, D3). Scale bar, 20  $\mu$ m. E1, Graph showing the number of coupled cells in the thalamus and hippocampus, depending on whether the injected cell was an astrocyte (AC) or an oligodendrocyte (OL). Size of the GJNs did not differ significantly. E2, The proportion of PLP-GFP+ cells in the networks was larger in the thalamus, but independent of the cell type initially filled with the tracer (TH,  $53.1 \pm 6.4$  % and  $66.5 \pm 8.4$ %, HC:  $12.4 \pm 1$  and  $13.4 \pm 1.4$ , injection into AC or OL, respectively). Number of experiments is given above bars. Asterisks indicate statistical significance.

188x346mm (299 x 299 DPI)

1  
2  
3  
4  
5  
6  
7  
8  
9  
10  
11  
12  
13  
14  
15  
16  
17  
18  
19  
20  
21  
22  
23  
24  
25  
26  
27  
28  
29  
30  
31  
32  
33  
34  
35  
36  
37  
38  
39  
40  
41  
42  
43  
44  
45  
46  
47  
48  
49  
50  
51  
52  
53  
54  
55  
56  
57  
58  
59  
60

For Peer Review



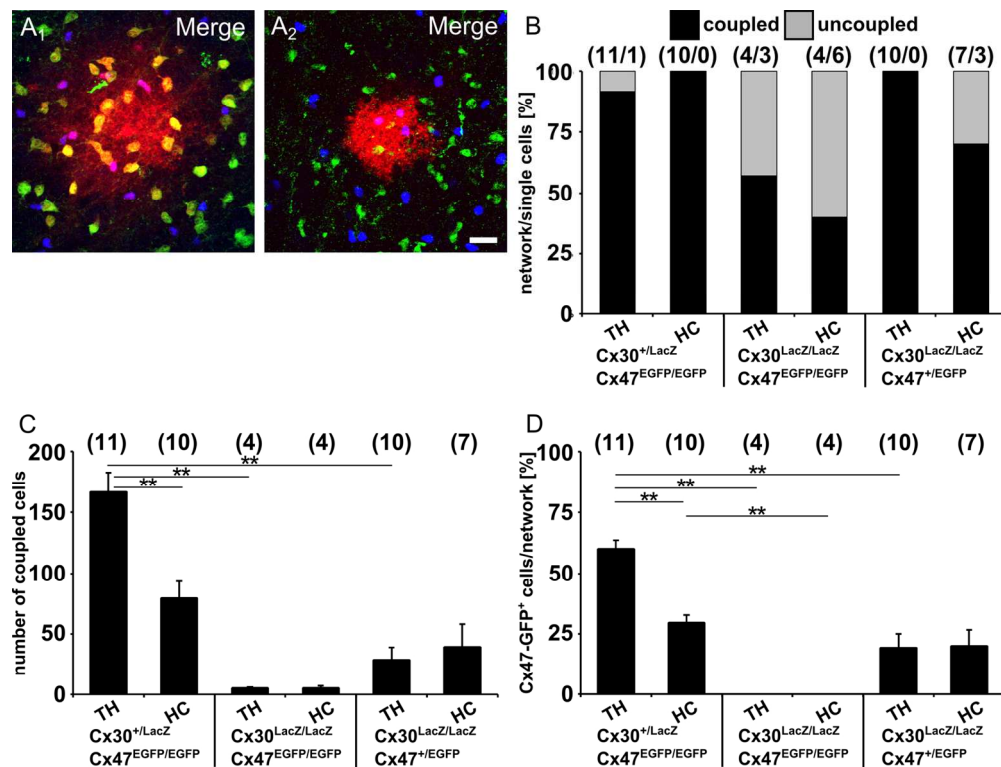
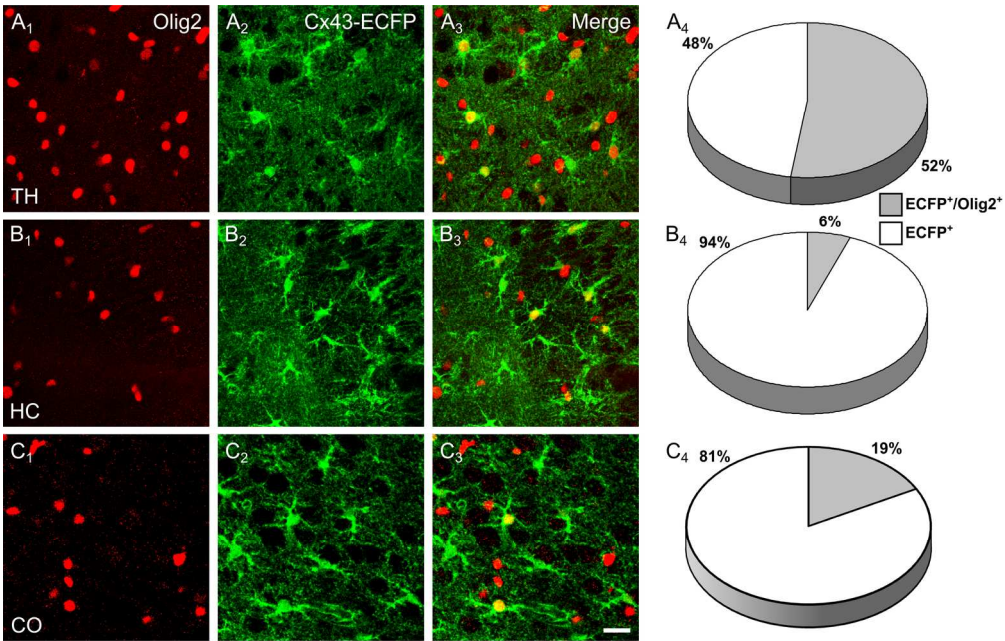
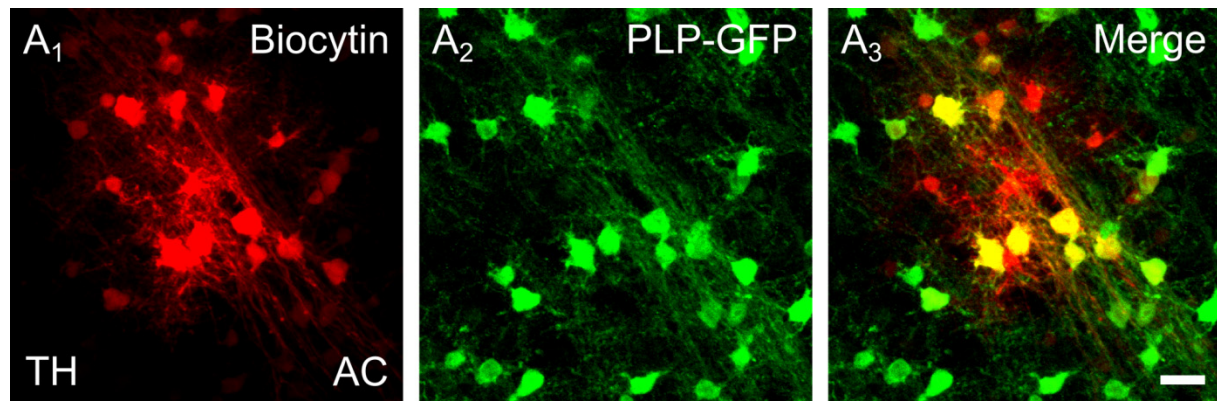


Figure 7. Panglial networks require Cx30 and Cx47 in the thalamus. Astrocytes in Cx30<sup>ki</sup>LacZ;Cx47<sup>ki</sup>EGFP mice were identified for tracer injection with SR101. Analysis of biocytin-filled networks (red) for the presence of Cx47-EGFP (green) and Cx30-LacZ (blue) expressing cells in Cx30<sup>+/LacZ</sup>;Cx47<sup>EGFP/EGFP</sup> mice revealed panglial networks (A1) while coupling was lacking or drastically reduced in homozygous Cx30<sup>LacZ/LacZ</sup>;Cx47<sup>EGFP/EGFP</sup> mice (A2). Examples depict networks in the thalamus. Scale bar, 20  $\mu$ m. (B) Three genotypes were analyzed both in hippocampus and thalamus for the proportion of coupled and uncoupled cells. (C) Analysis of network size revealed minimal tracer spread in Cx30/Cx47 deficient mice. (D) Proportion of Cx47-EGFP<sup>+</sup> oligodendrocytes. Note that oligodendrocytes were lacking in GJNs of Cx30/Cx47 deficient mice. Asterisks indicate statistical significance, number of experiments is given in parentheses.

150x114mm (299 x 299 DPI)

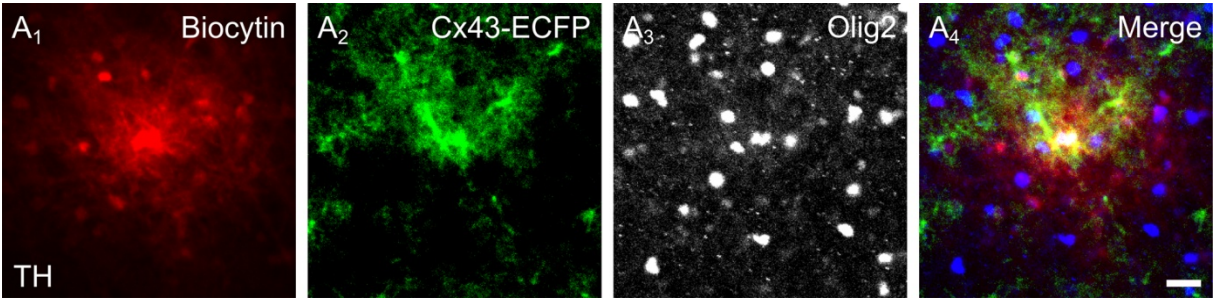


Thalamic Cx43-ECFP+ cells express the oligodendrocyte marker Olig2. Immunostaining for Olig2 in thalamus (A1) and hippocampus (B1) was performed in Cx43ECFP/+ mice (A2, B2). Merged images (A3, B3) show a large overlap of ECFP and Olig2 staining in the thalamus, while in the hippocampus only very few ECFP+/Olig2+ cells were observed. Scale bar, 20  $\mu$ m. A4, B4, Quantitative analysis of the ECFP and Olig2 expression profile confirmed a significant differences in the antigen profile of astrocytes in both regions (overlap TH,  $52.2 \pm 6 \%$ ; HC,  $6 \pm 1.8 \%$ ,  $n = 9$  for each region from 3 mice).  
180x115mm (299 x 299 DPI)

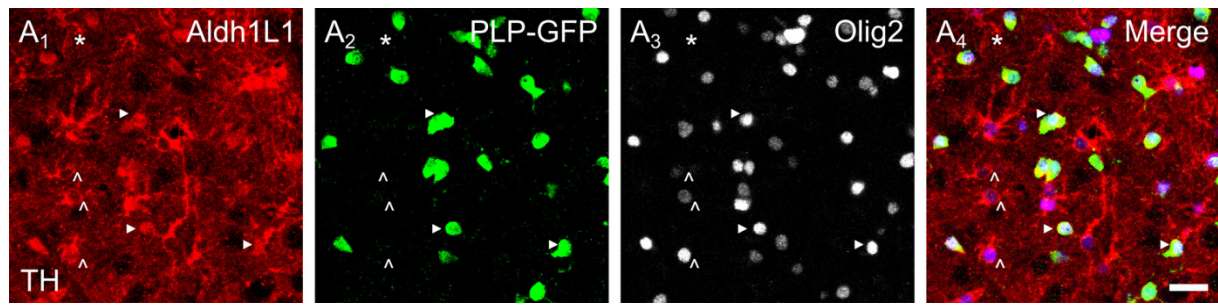


**Supplementary Figure 1: A:O coupling in juvenile (p9-p11) mice.** Astrocytes in the thalamus (TH) of PLP-GFP mice were identified by SR101 labelling (not shown). Astrocytes were tracer filled (A<sub>1</sub>, indicated by AC) and co-stained for GFP (A<sub>2</sub>) revealing diffusion of the tracer into PLP-GFP<sup>+</sup> oligodendrocytes (A<sub>3</sub>). Scale bar, 20  $\mu$ m.





**Supplementary Figure 2: Cx43-expressing cells in biocytin filled networks also express Olig2.** ECFP<sup>+</sup> astrocytes in the thalamus (TH) of Cx43<sup>ECFP/+</sup> mice were filled with biocytin (A<sub>1</sub>) and subsequently stained for Cx43-ECFP (A<sub>2</sub>) and Olig2 (A<sub>3</sub>). In the merged image the overlap of biocytin, ECFP and Olig2 is visible in two cells in the center of the network (A<sub>4</sub>). Scale bar, 20  $\mu$ m.



**Supplementary Figure: 3 Aldh1L1 is not a reliable marker for thalamic astrocytes.**

Immunostaining for Aldh1L1 (A<sub>1</sub>) was performed in PLP-GFP (A<sub>2</sub>) mice. Additionally, the transcription factor Olig2 (A<sub>3</sub>) was stained (blue in A<sub>4</sub>). Aldh1L1<sup>+</sup> cells express Olig2 at variable amounts (^) whereas some cells do not express Olig2 at all (\*). Unexpectedly, many PLP-GFP<sup>+</sup> cells were stained by Aldh1L1 antibodies (white arrow heads). Scale bar, 20  $\mu$ m.